YGS Open File 2025-6

# Geology and bedrock mapping updates at the Coffee Project gold deposit: implications for deposit classification

J.G. Kitchen[1], A.D. Brubacher*[1,2], J. Essman[1], F. Valli[1], P. Johansson[1], B. Kocay[1], J.L. Crowley[3] and K.P. Larson[4]

[1] Newmont Corporation - Coffee Project
[2] Yukon Geological Survey
[3] Boise State University
[4] University of British Columbia

Yukon

Published under the authority of the Department of Energy, Mines and Resources, Government of Yukon https://yukon.ca/en/department-energy-mines-resources.

Publié avec l'autorisation du Ministères de l'Énergie, des Mines et des Ressources du gouvernement du Yukon, https://yukon.ca/en/department-energy-mines-resources.



This, and other Yukon Geological Survey publications, may be obtained from:

Yukon Geological Survey
102-300 Main Street
Box 2703 (K-102)
Whitehorse, Yukon, Canada Y1A 2C6

email geology@gov.yk.ca

Visit the Yukon Geological Survey website at https://yukon.ca/en/science-and-natural-resources/geology.

In referring to this publication, please use the following citation:

Kitchen, J.G., Brubacher, A.D., Essman, J., Valli, F., Johansson, P., Kocay, B., Crowley, J.L. and Larson, K.P., 2025. Geology and bedrock mapping updates at the Coffee Project gold deposit: implications for deposit classification. Yukon Geological Survey, Government of Yukon, Open File 2025-6, 50 p. plus appendices.

Front cover: Coffee Project camp and airstrip, September 2019. Photo credit: Jacob Kitchen, Newmont Corporation.

Yukon

YGS Open File
2025-6

# Geology and bedrock mapping updates at the Coffee Project gold deposit: implications for deposit classification

J.G. Kitchen[1], A.D. Brubacher*[1,2], J. Essman[1], F. Valli[1], P. Johansson[1], B. Kocay[1], J.L. Crowley[3] and K.P. Larson[4]

[1] Newmont Corporation - Coffee Project
[2] Yukon Geological Survey
[3] Boise State University
[4] University of British Columbia

## Table of Contents

## Abstract

The Coffee Project comprises numerous gold occurrences, including the structurally-controlled gold-only Coffee deposit, which is hosted in poly-deformed Paleozoic basement rocks of the Yukon-Tanana terrane and Mesozoic plutons situated in the northern Canadian Cordillera, west-central Yukon. The deposit has been interpreted as having characteristics of numerous deposit types over the project's history including epithermal, reduced intrusion-related, Carlin-type, and orogenic gold, as well as combinations of deposit types. Recent mapping efforts and new geochronology highlight a previously unknown secondary phase of the Permian Sulphur Creek suite and led to the relocation of the Coffee Creek fault which is interpreted as a primary controlling structure of the Coffee deposit. A new structural analysis builds on previous depth estimates and suggests that the deposit formed at a relatively shallow depth of 1–3 km and together with the new map has outlined the structural history of the deposit in greater detail. New dike geochemistry suggests some mineralized Coffee dikes may be related to the Carmacks group volcanics or Prospector Mountain suite intrusives, which implies a Late Cretaceous age of formation. Field relationships and timing of regional faulting together corroborate a minimum age of formation of ~57 Ma. Available multi-element geochemistry highlights a subtle Au-As-Sb ± Ag-Pb-Te-W-Zn-K metal association that suggests a possible magmatic component to the mineralizing fluids at Coffee. Newly drilled shallow mafic intrusions adjacent to the Coffee Creek pluton serve as a potential source and may be coeval with movement on the Coffee Creek and Big Creek fault systems.

## Plain language summary

The Coffee Project in west-central Yukon includes several gold occurrences, the most significant being the Coffee deposit—a gold system hosted in faults and fractures that cut across metamorphic and igneous rocks ranging from approximately 400 to 67 million years old. This deposit does not fit neatly into commonly used classification schemes. Recent field work has led to a new geological map with updated faults and two new major rock units that were not observed before. Detailed analysis of the main gold-hosting faults at the Coffee deposit suggests the deposit was formed even shallower in the crust than previously thought (within ~1–3 km from surface). New work on gold-bearing igneous dikes highlights similarities to rocks in the Carmacks area that are known to be approximately 72–67 million years old. This means the gold may be as young as the Carmacks rocks, which is up to 29 million years younger than previously thought. The gold at this deposit is well known to be associated with arsenic and antimony, and recent work demonstrates that a subtle relationship with silver, lead, tellurium, tungsten, zinc, and potassium is more common than previously thought. The new metal associations, shallow depth, and young age all suggest that the deposit may be at least partly related to the unexposed igneous intrusions near the deposit that were found by recent drilling.

## Introduction

This report accompanies the updated Coffee Project geology map: Plate 1 in the Yukon Geological Survey (YGS) Open File 2025-5 (Kitchen et al., 2025).

The Coffee Project is located in the Dawson Range of western-central Yukon, Canada, approximately 130 km south of Dawson City (Fig. 1). The property lies within the Traditional Territories of the Tr'ondëk Hwëch'in and Selkirk First Nation, and the asserted traditional territory of the White River First Nation. The Coffee Project comprises the Coffee gold deposit (or 'Coffee') as well as numerous other gold mineral occurrences within the current Coffee property (defined by the Coffee Project claim block; Plate 1).

The earliest known bedrock mapping in the area was done in 1916 by D.D. Cairnes of the Geological Survey of Canada (GSC), as part of the Klotassin river map sheet, and to a lesser extent as part of the larger southwestern Yukon map sheet dated 1917 (Cairnes, 1917; Cairnes et al., 1917; Cairnes et al., 1918). The area was mapped again from 1970 to 1972 by Tempelman-Kluit (1973a, 1973b) as part of the Snag map sheet. Recent maps are based primarily on the Stevenson Ridge map sheets compiled by Ryan et al. (2013a, 2013b). Local refinements to Ryan et al. (2013a, 2013b) were completed on the property by Bartlett, (2016), Bartlett et al. (2016) and MacWilliam (2018). The current regional YGS map in the area is primarily based on Ryan et al. (2013a, 2013b), with additions from Sánchez et al. (2014). The accompanying updated geology map (Plate 1; Open File 2025-5) builds on and refines contacts and faults within the Coffee property and includes some minor edits to the current YGS map outside the property boundary.

Coffee is a structurally-controlled Au-only deposit hosted within Paleozoic metamorphic rocks and mid-Cretaceous granite of the Yukon-Tanana terrane (YTT; Fig. 1), and four mid- to (inferred) Late Cretaceous dike sets. For the purposes of this paper, the 'mid-' Cretaceous refers to ~115–90 Ma. The global gold resource at Coffee is 56 Mt at 1.22 g/t Au totalling 2.37 Moz Au (Newmont, 2023). Several authors have conducted work on the Coffee deposit including Wainwright et al. (2011), Cruikshank (2011), MacKenzie et al. (2013, 2014), Buitenhuis (2014), Boyce (2014), Buitenhuis et al. (2015), Bartlett et al. (2016), Bartlett (2016), Lee (2017) and MacWilliam (2018). These authors studied and described the fundamentals of the deposit, some of which are outlined and expanded upon in this study. The current consensus is that Coffee is an epizonal orogenic gold deposit emplaced at approximately 5 km depth at ~96 Ma (MacWilliam, 2018). This report summarizes 2022-2023 bedrock mapping updates, as well as new geochronology, geochemical analysis, and structural analysis. Based on these studies, a revised interpretation of the deposit is discussed, suggesting that the deposit instead formed related to Late Cretaceous (~72–67 Ma) intrusions at depths of only ~1–3 km.

### Exploration history

Early exploration work in the vicinity of Coffee commenced in the 1960s and 1970s following the discovery of the Casino copper-gold porphyry and continued into 1986 when the Geological Survey of Canada conducted regional-scale stream sediment sampling. Results from this survey did not produce any anomalous gold values from samples collected in the tributaries draining the main deposit, but elevated arsenic and antimony were noted. In 1999, Deltango Gold Ltd. conducted silt and soil geochemical sampling programs. Prospector International Resources Inc. also conducted silt and soil geochemical sampling programs in 1999 and 2000 and successfully delineated a Au-in-soil anomaly approximately 400 by 900 m on the eastern margin of Supremo (Jaworski and Meyer, 2000; Jaworski and Vanwermeskerken, 2001). No follow-up work was conducted by Deltango Gold Ltd. or Prospector International

Resources Inc. In 2006, Shawn Ryan staked the recently lapsed claims and conducted grid and ridge-top soil sampling utilizing Yukon Mineral Exploration Program (YMEP) grants issued by the Government of Yukon, outlining an extensive Au-in-soil anomaly (Ryan, 2007, 2008).

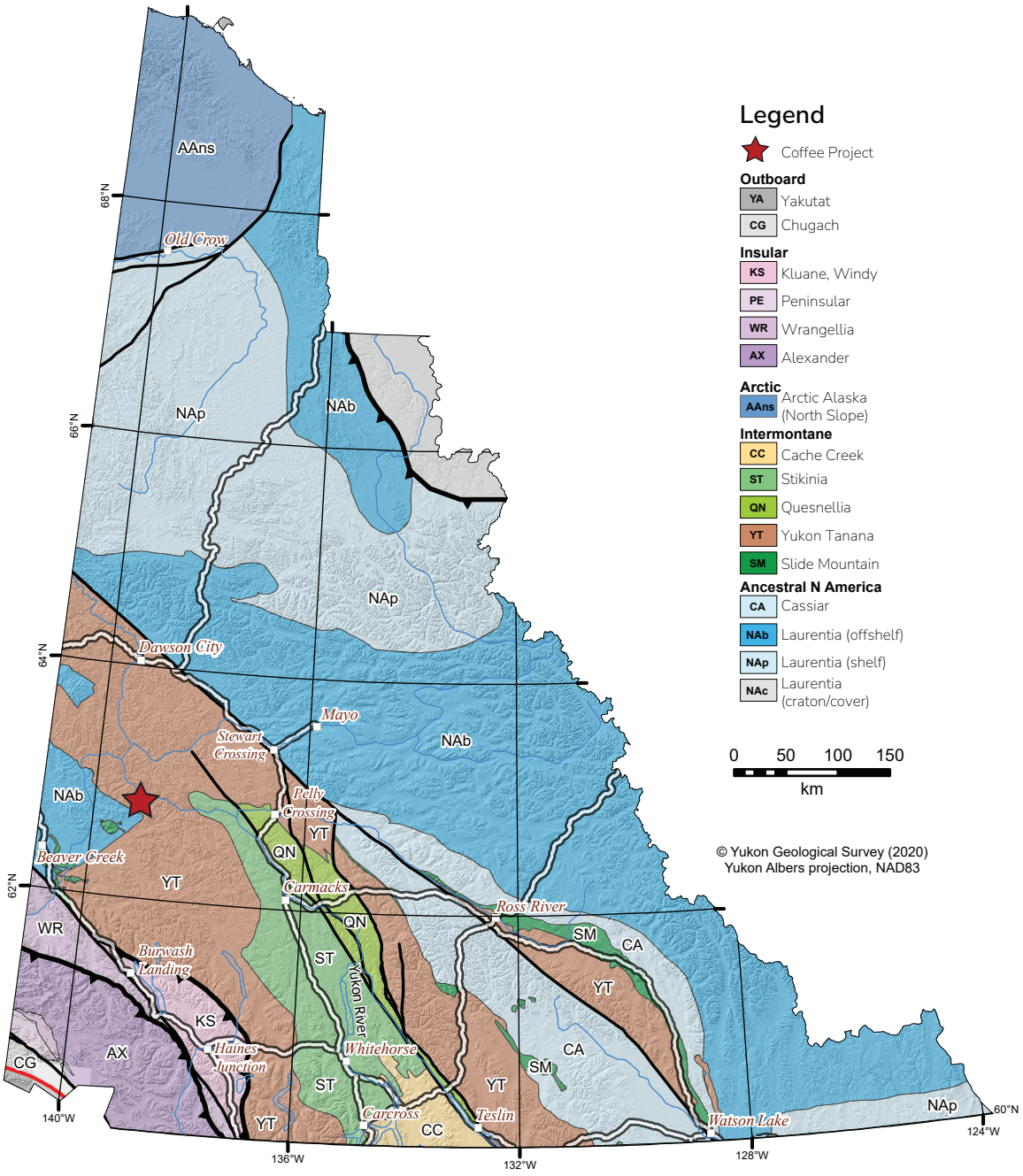


***Figure 1.*** *Terrane map of Yukon (Yukon Geological Survey, 2023c). The red star indicates the location of the Coffee Project.*

In 2009, Kaminak Gold Corporation entered into an option agreement with Shawn Ryan to acquire the Coffee Project. After the acquisition, the claim package was expanded and exploration continued with surface trenching and soil sampling over the initial Au-in-soil anomaly in the main deposit area (Doerksen et al., 2016). The first diamond drilling in 2010 led to the discovery of the Supremo, Latte, Double-Double, Kona and Americano zones (Plate 1;

Doerksen et al., 2016). Infill and exploration drilling continued from 2010 to 2012, along with initial metallurgical testing, leading to the first mineral resource estimate in 2013 (Chartier et al., 2013). Infill drilling and metallurgical testing continued to 2014, producing a Preliminary Economic Assessment (PEA), followed by a Feasibility Study in 2015 (Doerksen et al., 2016). Kaminak Gold Corporation was purchased in 2016 by Goldcorp Inc. who continued infill drilling into 2019. Since the acquisition of Goldcorp Kaminak Ltd. by Newmont Corporation in 2019, exploration, infill, and geotechnical drilling has continued up to the end of 2023.

Exploration work done on the project includes: property and deposit-scale mapping, geochemical soil and silt sampling, bulk leach-extractable gold (BLEG) and heavy mineral stream sediment sampling, biochemical sampling, ground and airborne geophysical surveys (VLF-EM, VTEM, ELF-EM, HLEM, Ohm Mapper, GPR, H-V and MASW seismic, magnetics, IP resistivity, gravity, and borehole EM), airborne radiometrics, trenching, reverse circulation drilling (365 112 m), rotary air blast drilling (2197 m), sonic drilling (156 m), and diamond drilling (242 242 m) which includes drilling for geotechnical purposes (3010 m).

## Regional geology

The Yukon-Tanana terrane is an allochthonous pericratonic terrane which has a protracted history of rifting, magmatism, and metamorphism spanning from the Late Devonian into the Mesozoic (Figs. 1 and 2; Colpron et al., 2006). Numerous orogenic and magmatic-hydrothermal mineral deposits occur throughout the YTT as a result of orogenesis and wide-spread magmatism in the Mesozoic. These events range from Late Triassic magmatism that produced Cu-Au mineralization such as Minto and Carmacks Copper (Kovacs et al., 2020), to Late Cretaceous porphyry systems such as Casino and Mount Freegold (Fig. 2; Allan et al., 2013). Orogenic deposits also occur over two distinct intervals: between 163 and 155 Ma (e.g., Golden Saddle; Bailey, 2013); and the mid-Cretaceous at 96 to 92 Ma, such as the Boulevard and Longline occurrences (Fig. 2; Joyce, 2002; Allan et al., 2013; McKenzie et al., 2013).

The Dawson Range is a west-northwest-trending topographic plateau in the YTT that remained unglaciated during the last ice age. In the Dawson Range the metamorphic rocks of the YTT consist of psammitic to semi-pelitic schists of the Snowcap assemblage, orthogneiss of the Sulphur Creek and Simpson Range suites, felsic to mafic metavolcanic and metasedimentary rocks of the Finlayson assemblage, micaceous schist of the Klondike assemblage, and undifferentiated ultramafic rocks (Plate 1; Ryan et al., 2013a, 2013b; MacWilliam, 2018). The metamorphic units are intruded by granite of the mid-Cretaceous Dawson Range batholith (DRB) and the Coffee Creek pluton (CCP), both of which are part of the Whitehorse plutonic suite (Ryan et al., 2013a, 2013b).

## Regional structures

Early-stage deformation in the Dawson Range is recorded by Late Triassic to Early Jurassic metamorphic foliation fabrics and thrust imbrication in the Snowcap and Klondike assemblages, as well as northeast-verging folds and associated crenulation fabrics (Allan et al., 2013; Colpron et al., 2022). This deformation is also recorded in the Permian Sulphur Creek suite, which is locally intercalated with the Snowcap assemblage.

The earliest stages of deformation are cut by faults of various orientations. North of the Coffee property the Yukon River thrust fault juxtaposes Late Devonian to Early Mississippian meta-igneous rocks of the Simpson Range suite on top of the pre-Late Devonian Snowcap assemblage (Plate 1; Ryan et al., 2013a, 2013b). The Yukon River thrust is broadly east-west

oriented and occurs roughly parallel to the Moose Creek fault , located south of the CCP (Fig. 2). The Moose Creek fault is interpreted as a major bounding structure between YTT rocks to the northeast and North American basement rocks to the southeast (Fig. 2). Large northeast-trending faults are identified in regional-scale maps, such as the Dip Creek fault (Fig. 2; Ryan et al., 2013a), and are interpreted as oblique-sinistral faults broadly coeval with Late Cretaceous magmatism (Allan et al., 2013). The Dawson Range is also affected by a network of broadly northwest-trending faults (Fig. 2), the most significant of which is the Big Creek fault (BCF) which runs for more than 150 km from the Mount Freegold area in the southeast past the Yukon River thrust in the northwest (Fig. 2). The Coffee Creek fault (CCF) intersects the BCF system to the east of Coffee property and has been interpreted to be cut by and perhaps dextrally offset by the BCF based on lineation interpretation of aeromagnetic data (MacWilliam, 2018; Yukon Geological Survey, 2023a; M. Colpron, pers. comm., 2024). The CCF has been interpreted as the primary controlling structure for the Coffee deposit (e.g., MacWilliam, 2018) with recent mapping updating the location and nature of the deposit-scale faults (see Discussion). Lastly, multiple north to northwest-trending faults are observed (Fig. 2); the dextral slip fault crosscutting the Moose Creek fault, the normal fault separating the DRB from Paleozoic metamorphic rocks southeast of Casino, and the normal fault dissecting the Prospector Mountain suite (Plate 1; Fig. 2).

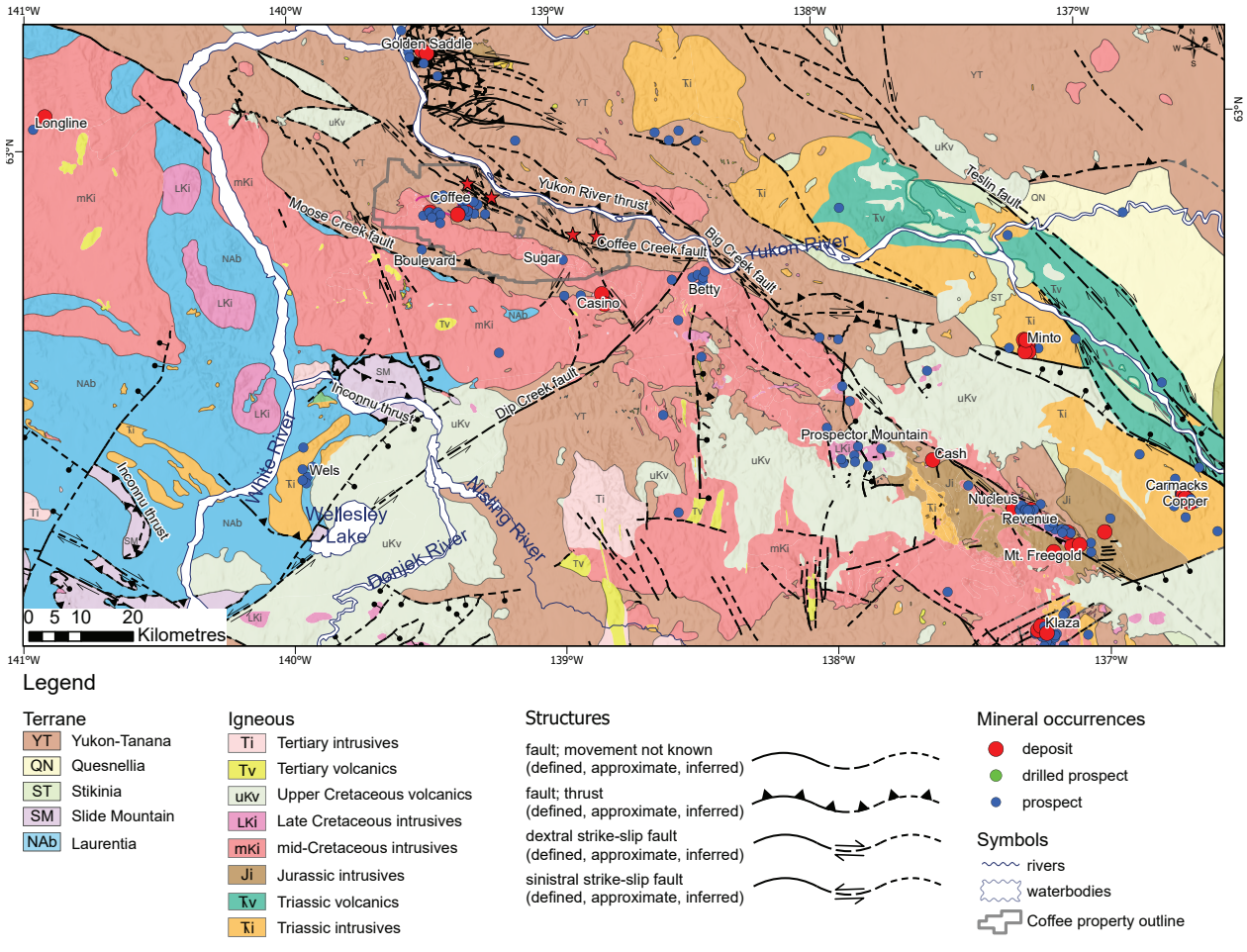


***Figure 2.*** *Overview geology map of the Dawson Range. Metamorphic and sedimentary rocks have been simplified into their respective terranes, with intrusive and extrusive igneous rocks overlain. Faults displayed are from this study and Yukon Geological Survey (2023a). Mineral occurrences are from MINFILE (Yukon Geological Survey, 2023a).*

## Methods

From 2020 to 2023, several studies were undertaken to improve the geological understanding of the Coffee deposit. These projects included field and desktop mapping, relogging of drill core from the Sugar prospect (Fig. 2), U-Pb geochronology, geochemical analysis of late intrusive phases and atypical gold mineralization, and structural analysis and reinterpretation of the main ore-controlling faults. Together these studies have further elucidated the geological and structural setting of the Coffee deposit during formation.

### Bedrock mapping

Updates to the Coffee property bedrock geology map were conducted using field mapping and a variety of desktop datasets including light detection and ranging (lidar), radiometric imagery, ground and airborne magnetics, and soil geochemistry. Many of the bedrock units on the property can be difficult to map due to the limited extent of bedrock exposures, therefore the use of additional datasets is necessary to create an accurate and reliable geological map. Desktop studies were conducted prior to each field season to identify map features in geochemical and remote sensing datasets that would be field-checked.

Bedrock mapping in the field consisted of numerous traverses over the 2022 and 2023 field seasons across the property (Plate 1). This work focused on investigating prominent topographic lineaments, refining contacts between the Snowcap assemblage, Sulphur Creek suite, and mid-Cretaceous granites across the property, and sample collection for geochronology (Fig. 3). Bedrock mapping was expanded beyond the traverse locations using several remote sensing datasets. K-Th-U radiometric imagery shows clear contrast between many bedrock units and was used extensively to map contacts and interpret faults beyond the limits of field mapping (Plate 1). Similarly, the property-wide lidar dataset provides high-resolution surface information that allowed for tracing bedding and faults away from field mapping locations. Geophysical imagery of ground and airborne magnetics was another means used to confirm plutonic-orthogneiss contacts from surrounding metasedimentary and metavolcanic rock packages. Soil geochemical data was interpreted using principal component analysis (PCA) and factor analysis studies to find patterns of elemental associations across the property. These methodologies were completed using IMDEX ioGAS (PCA) and TIBCO Statistica (factor analysis) software and the resulting data was reviewed in ESRI ArcGIS Pro to compare signatures of known bedrock units.

### Geochronology

A targeted geochronology program aimed to understand the nature of the newly discovered Upper Sulphur Creek unit found to the north of the main deposit area during 2022 mapping (Plate 1). Additionally the geochronology program aimed to obtain tighter constraints on the timing of mineralization by dating mineralized dikes that crosscut the well-constrained CCP and could therefore provide a more precise maximum age of mineralization.

Zircon U-Pb dating was conducted at the Isotope Geology Laboratory at Boise State University. Dates were obtained by laser ablation inductively coupled plasma mass spectrometry (LA-ICP-MS) following the methods outlined in Appendix A. Zircon geochronology tables are found in Appendix B.

Apatite U-Pb dating was conducted at the Fipke Laboratory for Trace Element Research (FiLTER) at the University of British Columbia - Okanagan. Dates were obtained by LA-ICP-MS following the methods outlined in Šilerová et al. (2023). Apatite geochronology tables are found in Appendix C.

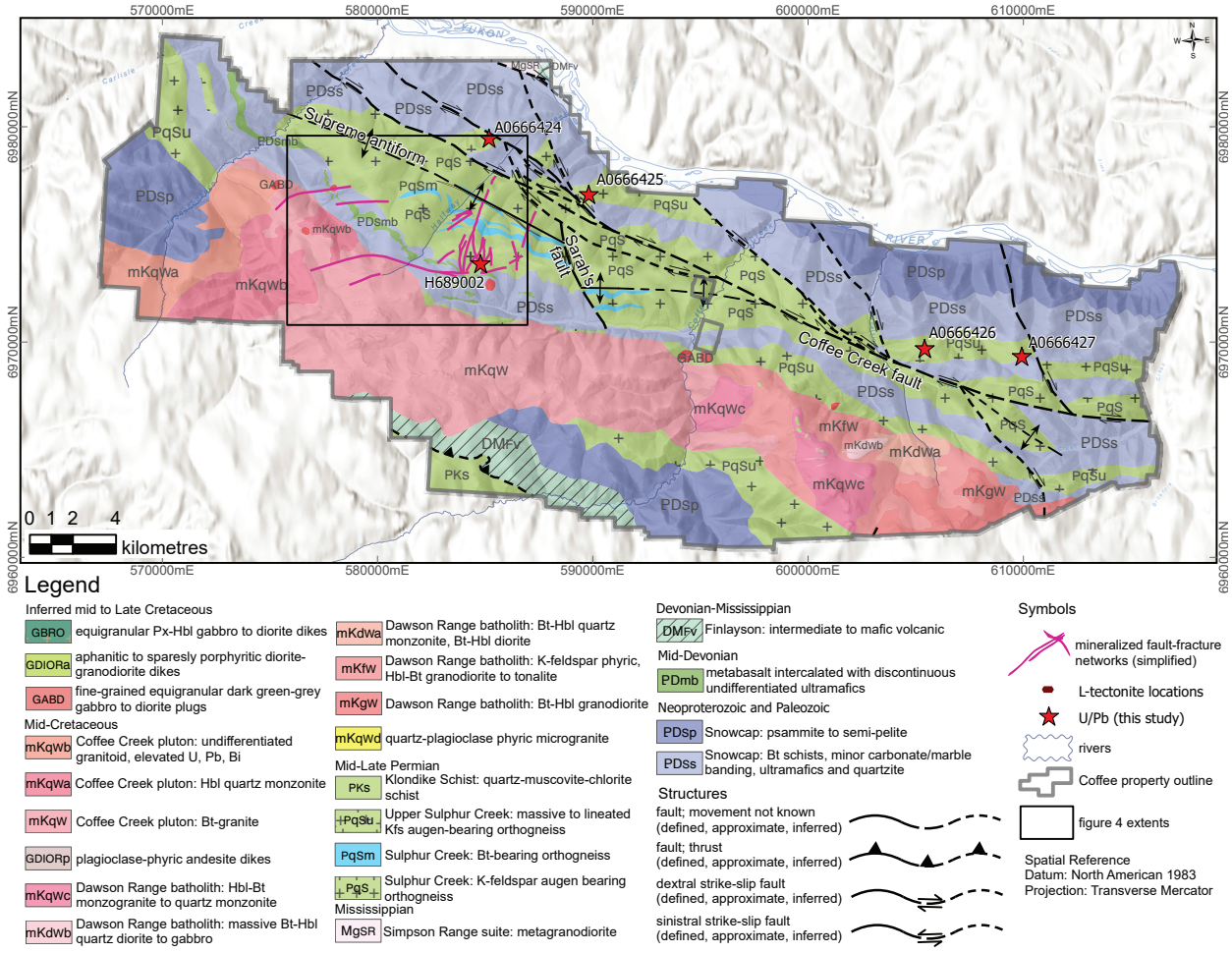


***Figure 3.*** *Simplified property geology map. Zircon U-Pb geochronology samples from this study displayed as red stars. The black box delineates the extents of Figure 4.*

## Geochemistry

Whole-rock geochemistry was used to compare dikes occurring at Coffee to dikes occurring elsewhere in the YTT. Twenty-one select fresh dike samples from Coffee were compared to a dataset of mid-Cretaceous Mount Nansen group rocks (n = 17; Klöcking et al., 2016), and also a dataset of Late Cretaceous Carmacks group volcanics (n = 18; Johnston et al., 1996). Geochemistry tables are found in Appendix D.

Additionally, four-acid digestion inductively coupled plasma mass spectrometry (ICP-MS) 61-element geochemistry was adopted at the Coffee Project in 2021. This was used to investigate alteration and metal associations in hole 23-MAC-DD055 where atypical mineralization styles are observed.

## Structural analysis

Using a 3D structural model of the Coffee deposit breccia corridors, a structural analysis was undertaken to reconcile the geometry of the mineralized fault zones with regional kinematic constraints and further assess the proposed depth of mineralization. This structural analysis was completed using MohrPlotter and Stereonet software (Allmendinger, 2023), the Coffee deposit 3D breccia model (Fig. 4), and rock mass characterization data.

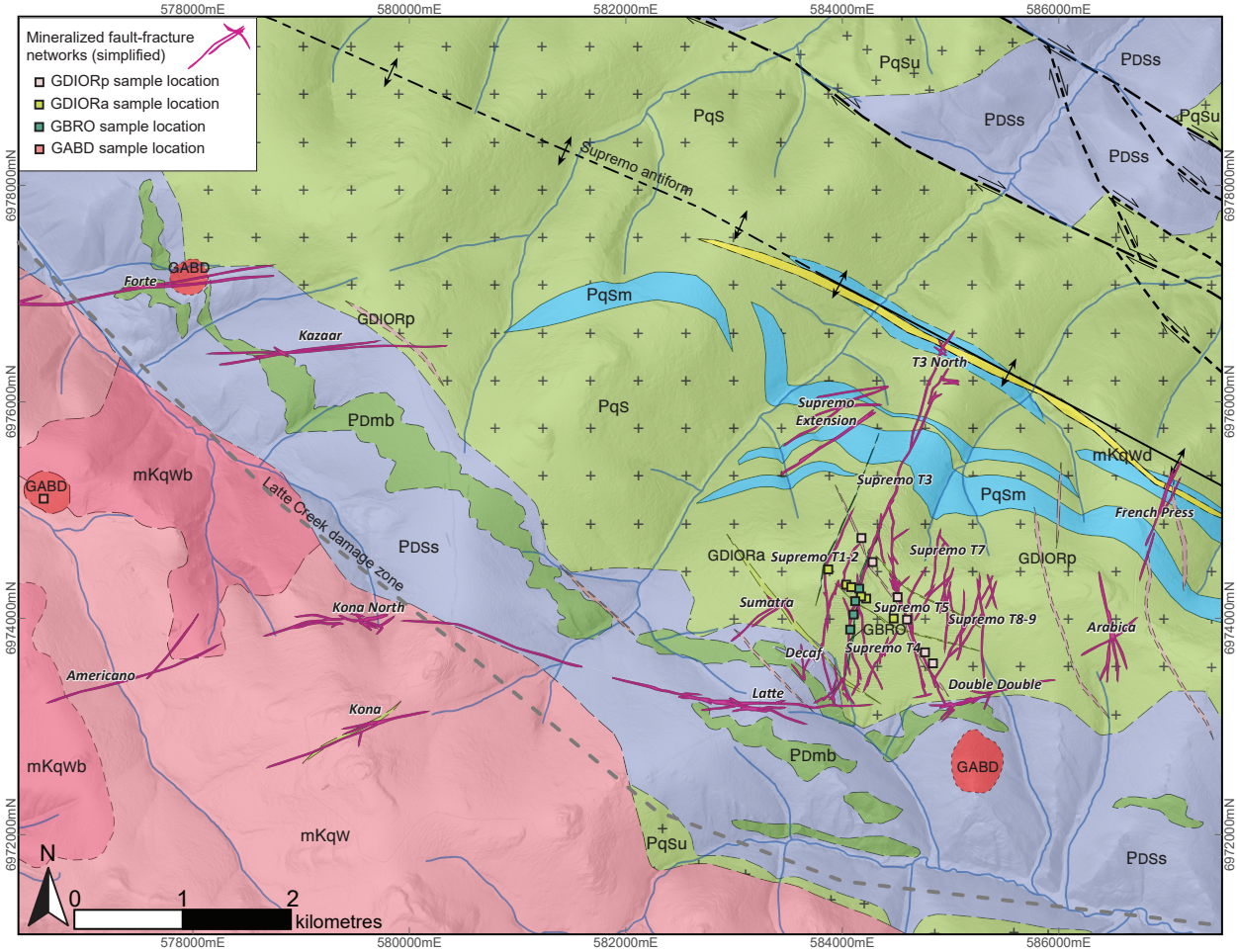


***Figure 4.*** *Overview of the main Coffee deposits. Mineralized fault-fracture networks represented in pink, with deposit and inventory zones/subzones labelled. Dike geochemistry sampling locations shown as coloured squares. See Figure 3 or Plate 1 for lithology legend.*

## Property geology

Twenty-two map units occur on the Coffee property (Plate 1; Fig. 3). The pre-Late Devonian meta-sedimentary rocks of the Snowcap assemblage are structurally overlying Late Permian meta-granitoid rocks of the Klondike assemblage, with the contact presumed to be a transposed intrusive contact (Plate 1; MacWilliam, 2018). Amphibolite and metabasalt occur at the base of the Snowcap assemblage, and undifferentiated ultramafic units occur as lenses throughout the assemblage (MacWilliam, 2018). Finlayson assemblage rocks are observed near the southern end of the property and stratigraphically overlie Snowcap assemblage psammite. The undeformed CCP intrudes the Paleozoic metamorphic assemblage, as do a series of Cretaceous mafic to felsic dikes (Fig. 4).

### Pre-Late Devonian Snowcap assemblage

#### *Semi-pelitic schist, marble and psammite (PDSs and PDSp)*

The Snowcap assemblage is divided into two property-scale units that are readily identified in outcrop mapping, soil lithogeochemistry and radiometrics. The dominant unit is a dark blue-grey to black, fine to medium-grained, strongly foliated muscovite-biotite schist with varying

abundances of millimetre-scale quartz and feldspar augen (Fig. 5a,b). The augen are typically foliaform, surrounded by aligned mica grains forming a penetrative metamorphic fabric (MacWilliam, 2018). Parallel with the penetrative foliation are intercalated lenses of pale pink to white marble and local, thin (1–50 cm) quartzite. Diopside, epidote, and magnetite occur locally within the schist, commonly proximal to lenses of marble and the main CCP (ibid.).

The second subunit of the Snowcap assemblage consists of dark blue-grey to black fine-grained, weakly foliated, compositionally banded psammite and minor pelite with local hornfels proximal to the CCP (Fig. 6).

### *Amphibolite and metabasalt (PDmb)*

Towards the structural base of the Snowcap schist package there are discrete and discontinuous lenses of dark blue-grey to green-grey fine to medium-grained, variably foliated amphibolite. These lenses are dominated by hornblende, biotite, and lesser quartz and feldspar (Fig. 5c). Chloritization of mafic minerals is common and epidote locally replaces hornblende (MacWilliam, 2018).

Metabasalt is also observed within the Snowcap schist as massive to banded lenses of striped to mottled dark green-grey to white fine to coarse-grained augite, biotite, chlorite, epidote and albite (Fig. 5d). Penetrative foliation is observed throughout and is defined by distinct compositional layering comprising strained albite, augite-biotite and chlorite bands (ibid.). Three-dimensional modelling of drillhole data and analysis of soil geochemistry data indicates that there are two major bands of this unit within the Snowcap package, with other minor lenses occurring near the Latte and Double-Double zones (Plate 1).

### *Paleozoic ultramafic rocks*

Throughout the Snowcap assemblage are discontinuous bodies up to 5 m wide of light grey and light to dark green-grey fine-grained talc schist, listwanite, serpentinite, and variably carbonate, magnesite, fuchsite, and epidote-altered rock (Fig. 5e; MacWilliam, 2018). Observed contacts between ultramafic rocks and surrounding schists are commonly sharp and typically crosscut the regional foliation at low angles. Lenses commonly display a strong to intense ductile shear fabric with locally observed recumbent folding. Intense and pervasive carbonatization and serpentinization completely destroy the primary mineralogy and texture of these rocks (ibid.).

## Devonian to Mississippian Finlayson assemblage (DmFv)

The Finlayson assemblage consists of moderate to strongly foliated dark green-grey amphibolite with fine-grained hornblende-biotite and trace garnet. Foliation within this unit is subvertical and foliation displays parasitic folding. These rocks are not observed in drill core and are not present in the main deposit area.

## Late Permian Klondike assemblage

### *Sulphur Creek suite – Supremo pluton (PqS)*

The K-feldspar augen-bearing orthogneiss of the Sulphur Creek suite (PqS; Plate 1; Fig. 5f), is pink-grey, medium to coarse-grained, and interlayered on a centimetre to metre-scale with medium blue-grey fine to medium-grained biotite-muscovite-feldspar-quartz schist (PqSm; Plate 1; MacWilliam, 2018). There is a main central panel of the augen orthogneiss, herein

called the Supremo pluton, and a structurally higher intrusion of the orthogneiss referred to here as 'Upper Sulphur Creek' (PqSu; Plate 1; Figs. 3 and 4).

Orthogneiss of the Supremo pluton is quartz-rich with 5 to 10 mm orthoclase augen, narrow bands of muscovite, and is locally affected by biotite and feldspar-destructive silicification and sericitization (MacWilliam, 2018). Red-pink hematite staining and disseminated brassy cubic pyrite occur throughout the unit (Fig. 5f). A penetrative planar fabric (S-tectonite) is present throughout most of the Sulphur Creek orthogneiss, defined by the alignment of mica grains and plastically deformed quartz + feldspar. Augen in the orthogneiss are typically symmetrical and are commonly observed to be replaced by quartz. The micaceous schist intercalations are compositionally very similar to the orthogneiss but contain less modal quartz and greater biotite (ibid.). The orthogneiss is also interlayered with narrow dark green orthoclase-porphyritic chlorite-epidote-quartz metagabbro dikes. These dikes intruded the orthogneiss unit prior to regional metamorphism and subsequent foliation (i.e., pre-Jurassic) and the contacts are parallel to foliation. A sample of the main unit of orthogneiss has a U-Pb zircon crystallization age of 263.7 ± 2.7 Ma (ibid.).

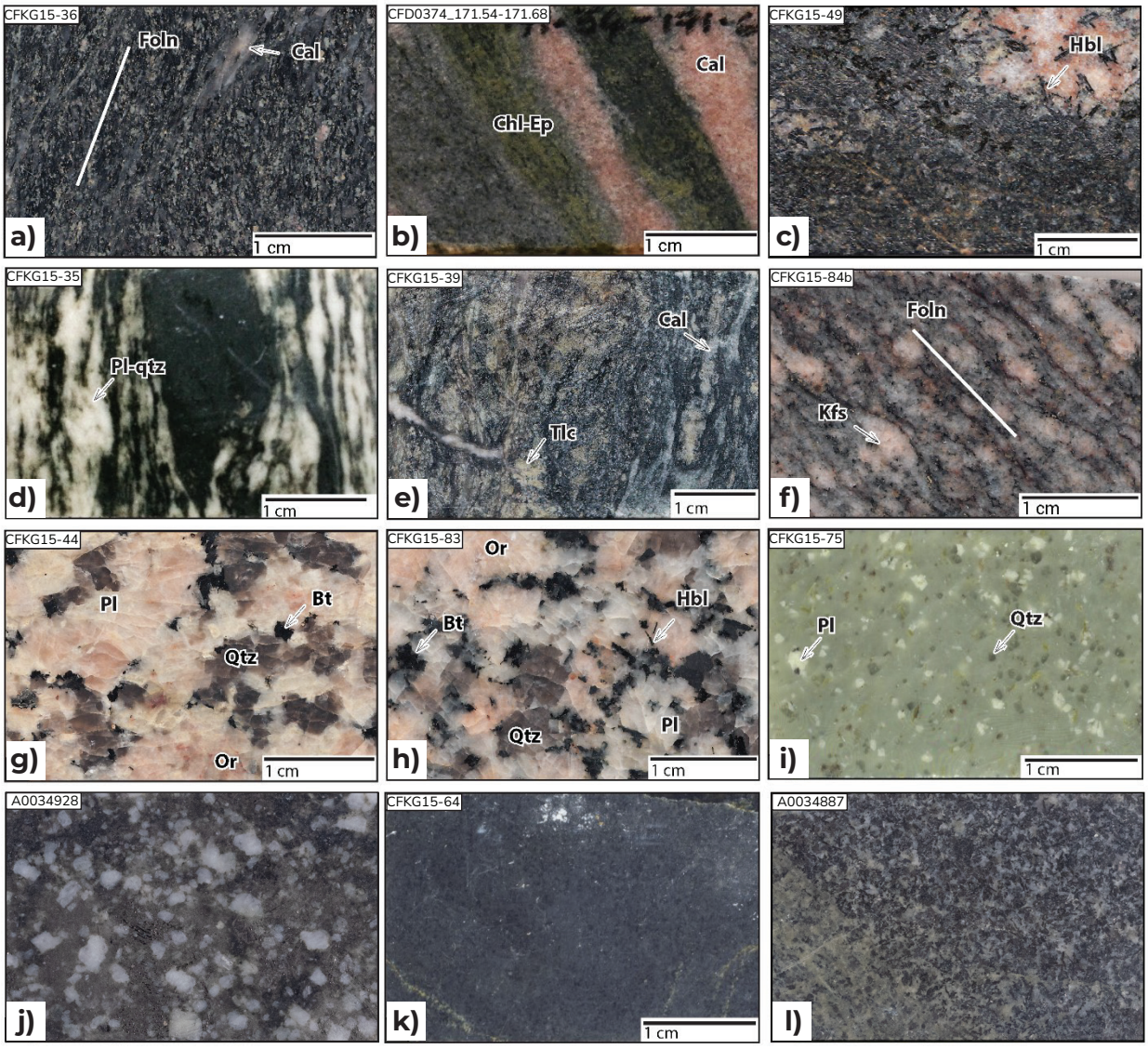


***Figure 5.*** *Representative sample photographs of lithologies observed on the Coffee property (adapted from MacWilliam, 2018).*


***Figure 6.*** *Representative hand sample photograph of the upper psammitic band of the Snowcap assemblage.*

### *Upper Sulphur Creek (PqSu)*

The previously unknown texturally distinct upper subunit of the Sulphur Creek suite was first mapped in 2022 and was not immediately recognized as being part of the Sulphur Creek suite. Local textural similarities and U-Pb dating in this study led to this conclusion (see Geochronology results ). This unit is separated from the main Supremo pluton orthogneiss unit by a panel of Snowcap assemblage and is observed on the northern limb of the Supremo antiform as well as truncating against the CCP on the southern limb of the antiform (Fig. 4). The subunit is mineralogically identical to the orthogneiss, however in addition to the typical S-tectonite textures it locally exhibits both an undeformed phaneritic texture and distinctive lineation fabric (L-tectonite) defined by elongated and plastically deformed feldspars (Fig. 7). All three textures are observed intermittently along strike of the unit.

### *Klondike Schist (PKf and PKs)*

Regionally, the Klondike Schist is mapped as a quartz-muscovite-chlorite schist (Yukon Geological Survey, 2023a). A single package of Klondike Schist overlies the mapped Finlayson assemblage in the southern portion of the Coffee property. Xenoliths of Klondike Schist are also observed within the CCP (Plate 1; Bartlett et al., 2016). These xenoliths are hundreds of metres wide and have strongly chlorite-altered contacts. These rocks are not observed in drill core and are rarely observed in outcrop on the Coffee property.

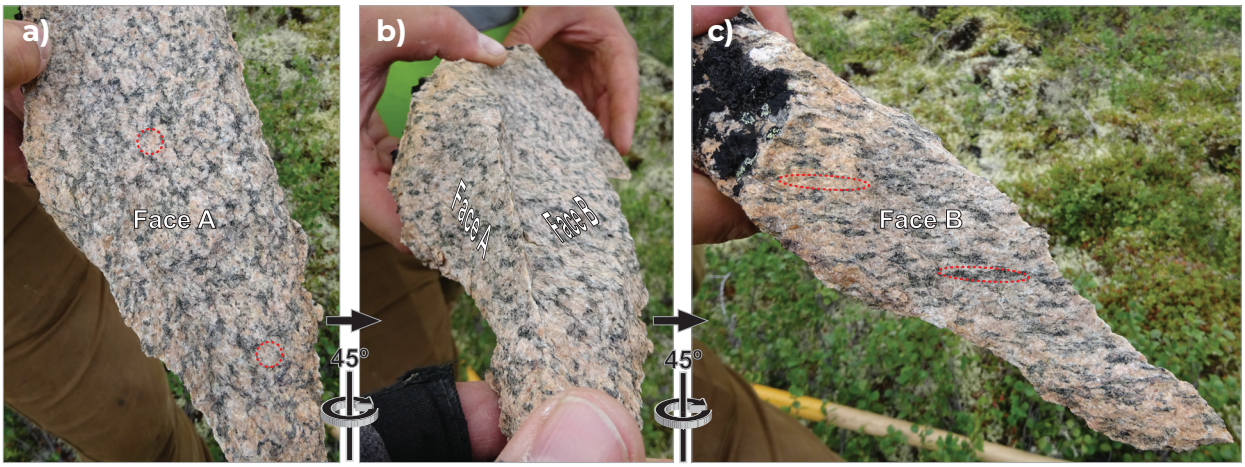


***Figure 7.*** *Representative hand sample photographs of the Upper Sulphur Creek unit with lineated texture (L-tectonite).* ***a)*** *(Face A) – view of L-tectonite hand sample looking down the elongated axis, with no observable deformation of crystals.* ***b)*** *the same hand sample rotated ~45° displaying Face A and Face B.* ***c)*** *(Face B) – the same hand sample fully rotated, looking perpendicular to the elongated crystal axis, demonstrating clear elongation of crystals.*

## Mid to Late Cretaceous plutonic rocks

### *Coffee Creek pluton (mKfw, mKdwa, mKdwb, mKdwc, mKqw , mKqwa, mKqwb, mKqwc)*

The mid-Cretaceous CCP is a composite pluton that intrudes the metamorphic rock package south of the Supremo antiform and forms a west-trending ridge south of the deposit where resistive outcrops and tors of granite are exposed (Fig. 3). This unit connects to the DRB southeast of the Coffee property near the Casino deposit and extends to the western edge of the Coffee property boundary (Figs. 2 and 3).

East of the Coffee Creek drainage there are five phases of mid-Cretaceous intrusions ranging from gabbro to monzogranite (Fig. 4). Dated units in this area pre-date the western portion of the CCP slightly with U-Pb zircon crystallization ages ranging from 110.9 to 104 Ma (Yukon Geological Survey, 2023b) which are closer in age to the DRB. Field mapping, drill core sampling and thin section analysis have allowed for mineralogical and geochemical differentiation of these intrusions, and their map pattern was extrapolated from this data using soil geochemistry, radiometrics and airborne magnetic datasets, building on mapping completed by Bartlett et al. (2016). The easternmost unit of the CCP is biotite-hornblende granodiorite which is the dominant lithology of the greater DRB (mKfw; Plate 1). The dominant intrusive phase in this section of the CCP on the Coffee property is a distinctive K-feldspar porphyritic hornblende-biotite granodiorite with minor quartz monzonite (mKfw; Plate 1). This unit hosts younger intrusive phases of biotite-hornblende quartz monzonite, biotite-hornblende quartz diorite to gabbro, and hornblende-biotite monzogranite (mKqwa, mKqwb, mKqwc; Plate 1). Large 10 to 100 m wide xenoliths of chlorite schist are hosted within the porphyritic granite and monzogranite intrusions (Plate 1). These xenoliths are interpreted as Klondike Schist (Bartlett et al., 2016). All plutonic rocks in this area of the property are crosscut by a series of biotite-hornblende, plagioclase-porphyritic diorite stocks and dikes as well as a poorly constrained series of basalt, andesite and pegmatite dikes.

West of the Coffee Creek drainage the CCP yielded dates ranging from ~103 to ~97 Ma (McKenzie et al., 2013; Buitenhuis, 2014; MacWilliam, 2018). Three phases are recognized within the CCP west of the Coffee Creek drainage; biotite granite (mKqw; Plate 1; Fig. 5g),

hornblende quartz monzonite (mKqwa; Plate 1; Fig. 5h), and an undifferentiated granite phase mapped primarily by remote sensing techniques (mKqwb; Plate 1). These three younger western phases of the CCP are collectively referred to as the Coffee Creek granite. All three phases are pink to pink-grey medium to coarse-grained, equigranular, and locally garnet and tourmaline-bearing. The biotite granite consists of quartz, alkali feldspar, plagioclase and biotite. The hornblende quartz monzonite has comparatively less modal quartz, equal proportions of alkali feldspar and plagioclase, and minor hornblende and biotite (Fig. 5g,h; MacWilliam, 2018). The undifferentiated granite phase is described from limited ground-truthing as medium to coarse-grained garnet + biotite granite with smoky quartz.

### *Cretaceous intrusions*

Five distinct phases of Cretaceous dikes and plugs intrude the metamorphic units; three of which also intrude the CCP (Fig. 4). Geochemically they are grouped as microgranite, diorite to granodiorite, and monzogabbro to gabbroic diorite (Fig. 5i,j,k,l; MacWilliam, 2018). Two phases of diorite dikes are observed: a porphyritic phase (Fig. 5j) and an aphanitic phase (Fig. 5k). All dikes are steeply dipping and crosscut the regional metamorphic foliation, striking east, north to northeast, and northwest (Fig. 4).

#### *Microgranite (mKqwd)*

The microgranite unit consists of white to beige altered feldspar and quartz phenocrysts in a cryptocrystalline quartz groundmass (Fig. 5i; MacWilliam, 2018). This unit is only observed at a few locations on the property, crosscutting the Sulphur Creek orthogneiss with an inferred northwest trend. This unit yielded a U-Pb zircon date of 115.6 ± 1.5 Ma (Table 1; ibid.), predating the CCP. The microgranite dikes are not mineralized due to unfavourable mineralogy.

***Table 1.*** *Existing isotopic age constraints on igneous samples from the Coffee deposit area prior to this study. *Unnamed samples quoted in Buitenhuis (2014) from unpublished data of Wainwright et al. (2010). The 'Cof' suite is used to denote samples occurring on the Coffee property with no exact regional correlative suite.*

| Sample ID | Easting | Northing | Lithology | Source | Suite | Mineral | Technique | Preferred age (Ma) | Error (2σ) |
|---|---|---|---|---|---|---|---|---|---|
| 99M-105 | 577775 | 6968097 | Coffee Creek granite | McKenzie et al. (2013) | CCP | zircon | LA-ICP-MS | 99.2 | 0.9 |
| 99M-107 | 560386 | 6973241 | Coffee Creek granite | McKenzie et al. (2013) | CCP | zircon | LA-ICP-MS | 99 | 0.3 |
| YGR-BV-002 | 573497 | 6968539 | Coffee Creek granite | McKenzie et al. (2013) | CCP | zircon | LA-ICP-MS | 99.5 | 0.7 |
| EB-01* | | | Coffee Creek granite | Buitenhuis (2014) | CCP | zircon | | 98.2 | 1.3 |
| EB-02* | | | Porphyritic diorite dike | Buitenhuis (2014) | Cof | zircon | LA-ICP-MS | 101.1 | 1.3 |
| MA15-CF6 | 585113 | 6973268 | Porphyritic diorite dike | Yukon Geological Survey (2023b) | Cof | zircon | LA-ICP-MS | 106 | 2.2 |
| CFD550 | 579718 | 6973044 | Aphanitic diorite dike | MacWilliam (2018) | Cof | zircon | LA-ICP-MS | 103.7 | 1.5 |
| CFKG15-13 | 582968 | 6973156 | Porphyritic diorite dike | MacWilliam (2018) | Cof | zircon | LA-ICP-MS | 103.1 | 0.8 |
| CFKG16-18 | 579717 | 6973044 | Coffee Creek granite | MacWilliam (2018) | CCP | zircon | LA-ICP-MS | 101.9 | 1.5 |
| CFKG16-87 | 574050 | 6972500 | Hbl Qz Monzonite | MacWilliam (2018) | CCP | zircon | LA-ICP-MS | 100.1 | 1.6 |
| CFKG61-77 | 585156 | 6976319 | Microgranite | MacWilliam (2018) | Cof | zircon | LA-ICP-MS | 115.6 | 2 |

#### *Porphyritic diorite to granodiorite (GDIORp)*

Plagioclase porphyritic diorite dikes consist of white, subhedral to anhedral plagioclase phenocrysts 1 to 5 mm in size that are hosted in a dark grey aphanitic matrix of microcrystalline quartz and feldspar (Fig. 5j). The abundance of feldspar phenocrysts varies from 1% (typically small phenocrysts) to ~20% (typically large and small phenocrysts). Patchy clay alteration overprints albite phenocrysts and the quartz-feldspar groundmass (MacWilliam, 2018). These dikes typically are subvertical and northwest-striking (Fig. 4). This dike phase yielded a U-Pb

zircon LA-ICP-MS date of 103.1 ± 0.8 Ma (Table 1; MacWilliam, 2018). Although not intimately spatially associated with mineralized trends the porphyritic diorite dike phase is weakly mineralized near mineralized fault/breccia corridors.

*Aphanitic diorite to granodiorite (GDIORa)*

The aphanitic diorite to granodiorite is dark grey to light grey, fine-grained, and equigranular, consisting of plagioclase + biotite + quartz ± hornblende ± pyrite with chlorite and rare epidote alteration of biotite, and clay, and carbonate alteration of plagioclase (Fig. 5k). Occasionally plagioclase, biotite, and pyrite appear as sparse phenocrysts. MacWilliam (2018) dated a sample of this unit that crosscuts the CCP; however, it only yielded zircons that were slightly older than the oldest Coffee Creek granite dates (103.7 ± 1.5 Ma; Table 1) and were thus interpreted as inheritance. This unit therefore still lacks a reliable geochronological age. The GDIORa dikes trend northwest to northeast, and commonly are gold-bearing when occurring along mineralized fault-breccia corridors.

*Monzogabbro (GBRO)*

The monzogabbro dikes are typically dark grey or green to black, fine-grained, and equigranular, consisting of plagioclase + hornblende + biotite + pyroxene ± pyrite with chlorite replacing biotite and clay/carbonate replacing plagioclase (Fig. 5l; MacWilliam, 2018). Individual grains are subhedral to euhedral and range from 1 to 3 mm. Bladed hornblende is present in coarser-grained samples, giving a speckled appearance with interstitial plagioclase (ibid.). Some occurrences of the gabbro are porphyritic with sparse fine-grained plagioclase phenocrysts. This unit sometimes has strong shear fabrics along contacts defined by aligned biotite crystals and abundant carbonate stringers, interpreted as syn-emplacement deformation and subsequent alteration respectively. The gabbro dikes frequently occur within mineralized corridors trending north-northwest to northeast and are commonly strongly mineralized themselves.

*Gabbroic diorite (GABD)*

A single narrow stock of dark grey to black, fine-grained, locally plagioclase porphyritic gabbroic diorite is observed within the CCP (Figs. 3 and 4). This intrusion was originally inferred through airborne magnetic geophysical surveys and then confirmed by subsequent surface drilling in 2023. Similar geophysical anomalies are observed across the property which are interpreted to represent other shallow, unexposed intrusions (Plate 1; Figs. 3 and 4). The geochemical name of gabbroic diorite (Middlemost, 1994) is used because mineralogical studies on this unit have not been conducted since the only samples are from RC drilling.

## Deposit structural setting

The host rocks at Coffee were deformed by a series of YTT-wide Paleozoic tectonic events, as well as Cretaceous deformation (e.g., Nelson et al., 2013; MacWilliam, 2018). Shallow south-southwest-dipping compositional layering ($S_0$) is observed locally within schist of the Snowcap assemblage, and as layers of marble and quartzite (MacWilliam, 2018). Tectonic foliation ($S_1$) formed parallel to $S_0$ during a flattening episode ($D_1$) likely in the Early Jurassic (Colpron et al., 2022). The $S_1$ fabric is axial planar to the earliest phase of folding ($F_1$) observed, which consists of tight to isoclinal folds (MacWilliam, 2018). This schistosity is defined by alignment of biotite and muscovite in mica-bearing units and by hornblende in metagabbro (ibid.). Quartz veins interpreted as metamorphic segregations or transposed early quartz veins also help define this schistosity (ibid.).

Following the development of the early $D_1$ fabrics, the regional $S_1$ metamorphic fabric was broadly folded into the Supremo antiform ($F_{2b}$; Fig. 3). Foliation measurements in drill core from the southern limb indicate $S_1$ dips shallowly (~30°) to the southwest, steepening slightly towards the south in the Latte area. To the north of the Coffee deposit the fabric in the northern limb dips moderately to the north-northeast and similarly becomes steeper in proximity to the Yukon River. The axial trace of this $F_{2b}$ antiform has largely been inferred from $S_1$ measurements in core but can be observed in exploration trenches north of the main deposit and in outcrop in Coffee Creek.

The undeformed mid-Cretaceous CCP intrudes the metamorphic units. The Cretaceous dikes are also largely undeformed, apart from minor shearing along the contacts of the monzogabbro and aphanitic diorite dike phases. These Cretaceous dikes are spatially associated with subvertical fault-fracture networks that are the primary controls of mineralization at Coffee. These faults are interpreted as high-order structures related to the CCF (e.g., MacWilliam, 2018).

## Mineralization and alteration at Coffee

The mineral endowment at Coffee is hosted within several zones each with varying host rocks and structural orientations. The bulk of the mineral resource occurs within the Supremo zone which is predominantly hosted within augen-bearing orthogneiss of the Sulphur Creek suite (Fig. 4). The Supremo zone is further broken down into different 'T'-structures named after exploration trenches (T1 through T9, excluding T6); the most significant of which is T3 which trends north-northeast and extends for approximately 5 km of strike length (Fig. 4). The Supremo T-structures are mostly north-northwest to northeast-trending and form an interconnected array of fault-fracture networks (Fig. 4). The Latte and Double-Double zones are located south of Supremo and each consist of nearly east-west trending structures that crosscut psammitic to semi-pelitic schists of the Snowcap assemblage (Fig. 4; MacWilliam, 2018). The T-structures intersect Latte and Double-Double south of the Snowcap-Sulphur Creek contact. The Kona and Kona North zones are the main bodies of mineralization hosted within the CCP. These zones consist of east-northeast trending fault-fracture networks (Fig. 4). Other mineralized zones at Coffee are situated in east-west trending fault fracture networks like Kazaar, Forte and Americano; north-northwest to north-northeast trending structures like Arabica, Decaf and French Press; and northeast trending structures like Supremo Extension and Sumatra (Fig. 4). Other mineral occurrences within the Coffee property that are more distal to the Coffee deposit, such as the Sugar occurrence, are not discussed in detail in this paper.

Gold at Coffee occurs as fine-grained auriferous pyrite, arsenopyrite and arsenian pyrite (e.g., MacWilliam, 2018). Ore is controlled by subvertical fault-fracture networks, characterized by variably mature, polyphase tectonic fault gouge and fault-fill breccias and cataclasites (Fig. 8; MacWilliam, 2018). These brittle structures range in deformation intensity from angular clast-supported crackle breccias to intensely milled fault gouge. The mature, gouge-rich breccias represent the centre of these fault-fracture networks, or 'fault core', whereas the less mature crackle breccias are typical of the edges of these fault-fracture networks, or 'damage zones', using the terminology of Sibson (2003). Quartz-carbonate cement is present in some degree within the matrix of some tectonic breccias; however, textures indicated that the quartz-carbonate fluid is infilling the breccia and did not play a major role in hydrothermally fracturing the rock. There is a notable lack of quartz or carbonate veining associated with the mineralizing fault corridors, however, rarely sulphide minerals can be associated with quartz-dolomite gangue as part of the quartz-rich breccias (e.g., Buitenhuis, 2014; Buitenhuis et al.,

2015; MacWilliam, 2018). Competent Fe-carbonate and quartz-carbonate cemented breccias occur sporadically in the fault zones but are volumetrically minor and exhibit no clear spatial correlation. Fe-carbonate-rich breccias are post-mineralization (e.g., Buitenhuis, 2014). In addition to fault-controlled gold mineralization, ore minerals also occur disseminated in the wallrock immediately surrounding these fault arrays (Figs. 8 and 9). Supergene oxide ore has been the focus of exploration since Coffee's discovery and occurs as limonite-hematite-goethite at depths of up to ~400 m and affects all styles of hypogene mineralization described above (Buitenhuis, 2014; Buitenhuis et al., 2015; MacWilliam, 2018).

Lithology also acted as a primary control on mineralization at Coffee, as mineralization favours Fe-rich units containing pyrite and biotite (Figs. 8 and 9; MacWilliam, 2018). In Latte and Double-Double, the dominant lithology is the Snowcap assemblage biotite schist. Since

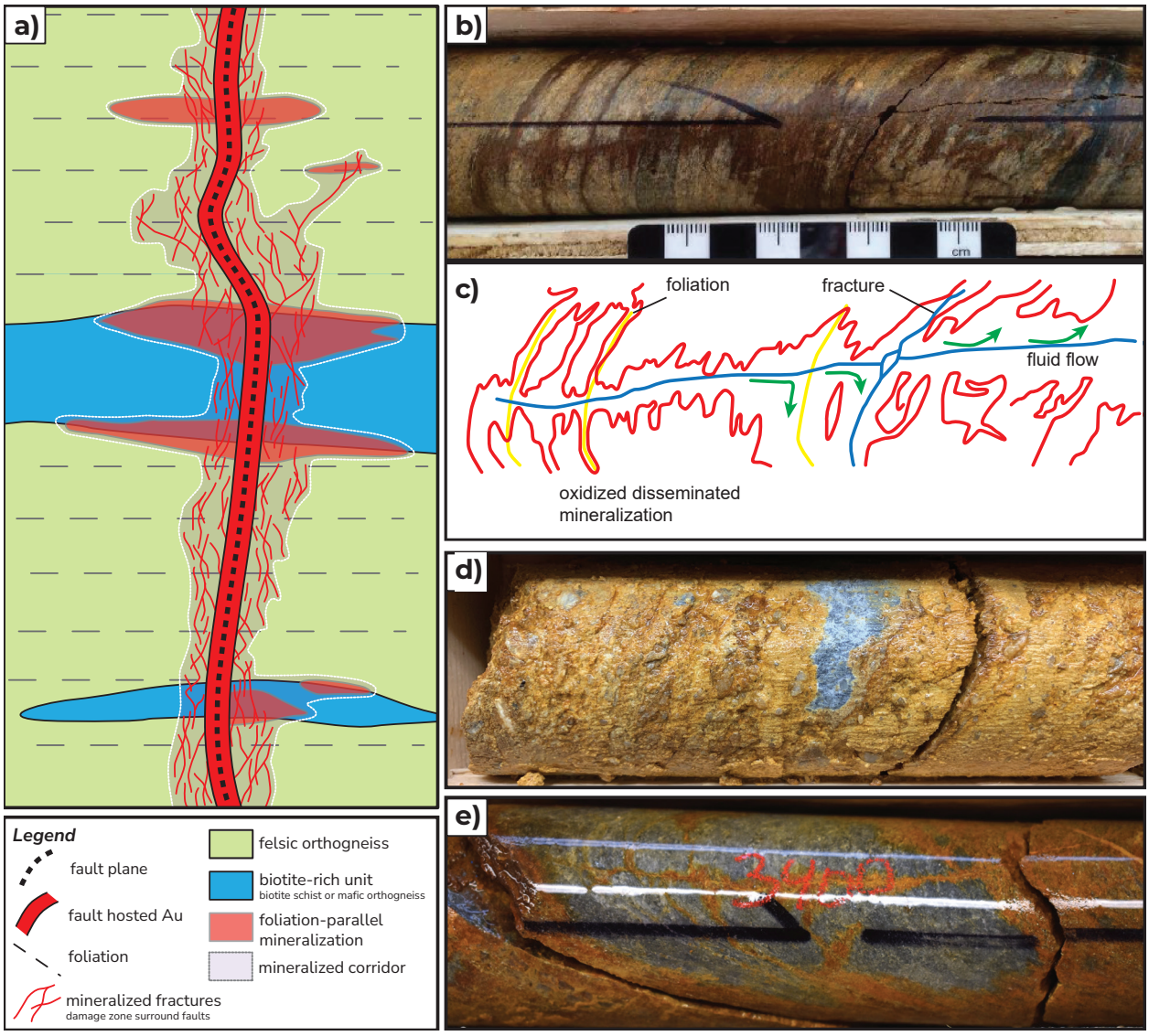


***Figure 8. a)*** *Idealized diagram of vertically oriented fault and fracture-hosted mineralization at Coffee. Diagram shows the controlling mineralized fault (black dashed line surrounded by red) with mineralized fracture network and foliation parallel wallrock-replacement mineralization. The pattern outlined in the diagram is fractal and thus can represent both zone-scale and drillhole-scale.* ***b)*** *Latte drill core showing foliation-parallel wallrock mineralization and oxidation away from a mineralized fracture (modified from MacWilliam, 2018).* ***c)*** *Sketch interpretation of oxidation pattern in part b (modified from MacWilliam, 2018).* ***d)*** *Mature gouge-rich breccia from core of a mineralized fault zone Supremo drill core.* ***e)*** *Immature crackle breccia/ fracturing from the damage zone of a mineralized fault zone.*

there is more iron available in biotite-rich units for mineralizing reactions, disseminated mineralization tends to extend farther into the wallrock from the controlling fault zones (up to 20 m in Latte zone; MacWilliam, 2018). In these zones sulphidation reactions consume Fe-bearing micas and produce foliation-parallel white mica + illite + arsenian pyrite pseudomorphs (Buitenhuis, 2014; MacWilliam, 2018). In contrast, disseminated mineralization adjacent to controlling structures in the relatively biotite-poor Sulphur Creek orthogneiss (Supremo zone) and CCP (i.e., Kona zone, Fig. 4) tends to reach 5 to 10 m into the wallrock (MacWilliam, 2018). Additionally, high-grade gold mineralization occurs along the intersection lineation between biotite-rich bands in the Sulphur Creek orthogneiss and mineralized fault-fracture networks (Fig. 9). The fault-fracture networks are also exploited by gabbroic and granodioritic dikes which themselves are commonly brecciated and mineralized (Fig. 4; MacWilliam, 2018).

Alteration at Coffee typically consists of white mica + illite + kaolinite + quartz + ankerite (Wainwright et al., 2011; Buitenhuis, 2014). Arsenopyrite, stibnite, realgar and native arsenic are also observed locally within mineralized zones in minor abundances (MacWilliam, 2018). White micas, as interpreted from available short-wave hyperspectral analyses, consist of $NH_4$ white mica, paragonitic muscovite and muscovite in mineralized zones (Fig. 10; MacWilliam, 2018). Available data suggests some concentric zonation of $NH_4$ white mica and paragonitic

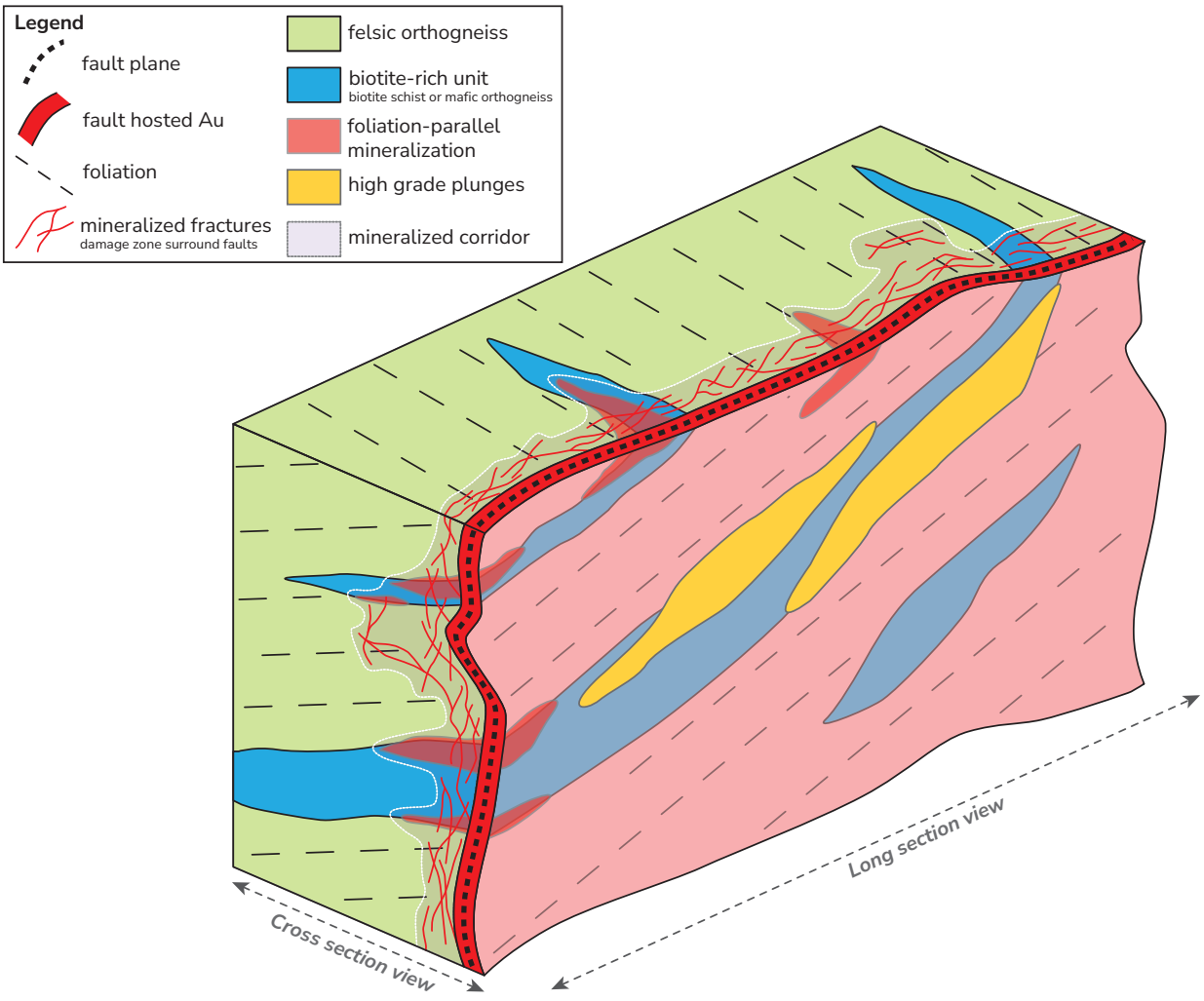


***Figure 9.*** *Idealized block diagram showing the cross section and long section views of mineralized brittle fault structures (as in Figure 8) and a long section view looking perpendicular to the structure. High-grade lenses (yellow) plunge down the intersection lineation of Fe-rich lenses (blue) and the main Au-bearing fault-fracture structure (red).*

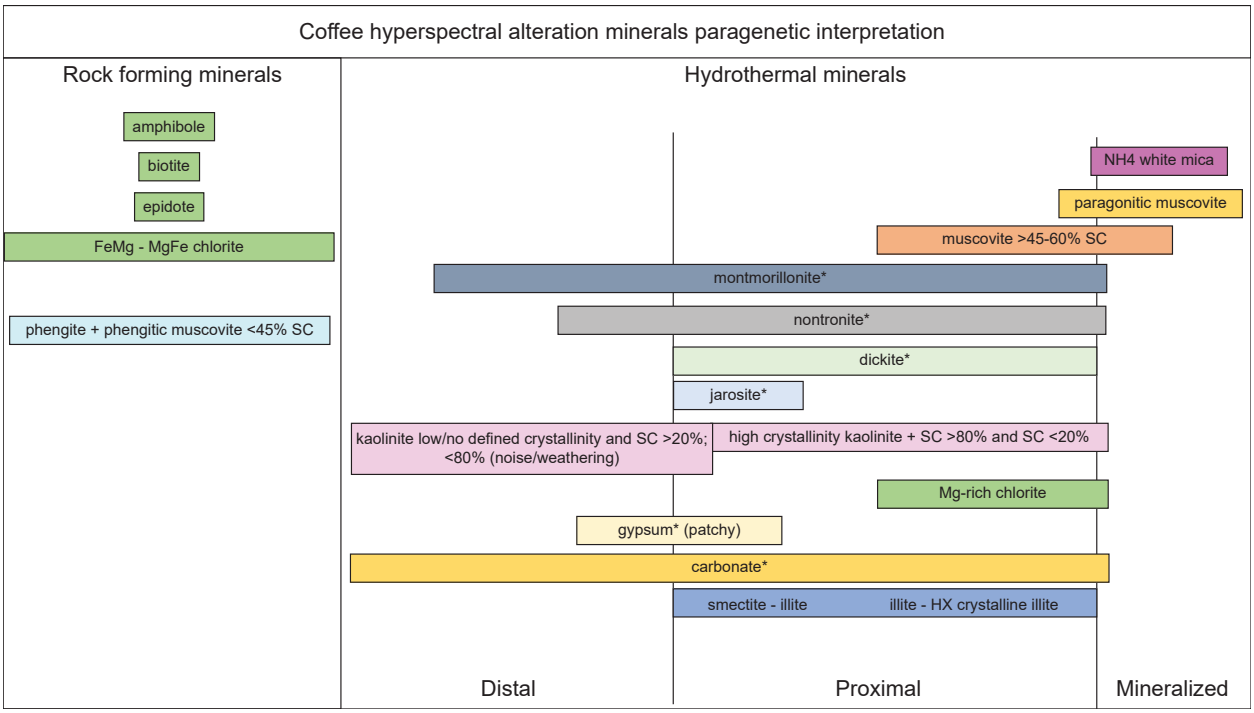


***Figure 10.*** *Hyperspectral alteration mineral paragenesis. Alteration and oxidation minerals identified from alteration modelling that signify pre-, syn- and post- (weathering) mineralization at Coffee. *These minerals had only minor spectral contributions. Additionally, carbonate type is undetermined due to low number of samples (unpublished Newmont study).*

muscovite may exist in mineralized zones (Fig. 11). No other vertical or horizontal alteration zonation is documented at Coffee.

Arsenic is intimately associated with gold at Coffee as the gold is hosted within arsenian pyrite (e.g., Wainwright et al., 2011; Buitenhuis et al., 2015; MacWilliam, 2018). Antimony is also used as an indicator of gold as it occurs as stibnite and within arsenian pyrite (MacKenzie et al., 2014). Sodium and potassium are observed to decrease with increasing gold mineralization as a result of the alteration of biotite, phengite and feldspar to the alteration assemblage of white mica and kaolinite (MacKenzie et al., 2014).

## Deposit model overview

Over the project's history, it has been stated that the Coffee deposit shares similarities with low-sulphidation epithermal, reduced intrusion-related, Carlin-type (and 'Carlin-like'), orogenic gold deposits, and a combination of these (Cruikshank, 2011; Chartier et al., 2013; Buitenhuis et al., 2015; MacWilliam, 2018). 'Carlin-like' is not a formally defined term but is often used to describe gold deposits that share some, but not all, characteristics of Carlin-type deposits. Allan et al. (2013), Buitenhuis (2014), and MacKenzie et al. (2014) suggested that Coffee resembles an epizonal orogenic gold system based on similarities to nearby prospects (i.e., Boulevard). Whereas other studies, as early as 2013, interpreted Coffee to be at least partially an epithermal gold deposit despite lacking typical characteristics such as a Ag ± Pb-Zn association and quartz + adularia veins (Cruikshank, 2011; Chartier et al., 2013; Buitenhuis et al., 2015). Buitenhuis et al. (2015) described 'epithermal-like textures' and interpreted them as an overprinting epithermal stage of mineralization, or the latest stages of a single evolving epizonal orogenic system. MacKenzie et al. (2013) also described sooty-sulphide-bearing veins with prismatic quartz and banded carbonate veins that crosscut the main mineralizing phase in

Latte and Double-Double but did not suggest that these represent an epithermal environment.

In more recent work, MacWilliam (2018) states that Coffee is an epizonal orogenic gold deposit, with the CCF acting as the main fluid conduit. The Coffee gold mineralization was interpreted to be deposited at a maximum depth of ~5 km following the emplacement of the mid-Cretaceous CCP, with a mineralization age of 97–93 Ma interpreted from $^{40}Ar/^{39}Ar$ dating of hydrothermal sericite and fuchsite (MacWilliam, 2018). A maximum age of gold deposition was demonstrated by the CCP crystallization age of 103-99 Ma, which also hosts mineralized fault-fracture networks in Kona and Kona North (Fig. 4; ibid.). MacWilliam (2018) also acknowledged that mineralization could be as young as ~57 Ma based on the inferred post-mineral deposition of the Rhyolite Creek volcanics near the Coffee property; however, 97–93 Ma has become the most cited age range of the deposit. Rapid exhumation rates of 2.0-3.5 km/Myr were inferred based on the depth and timing of mineralization, and an

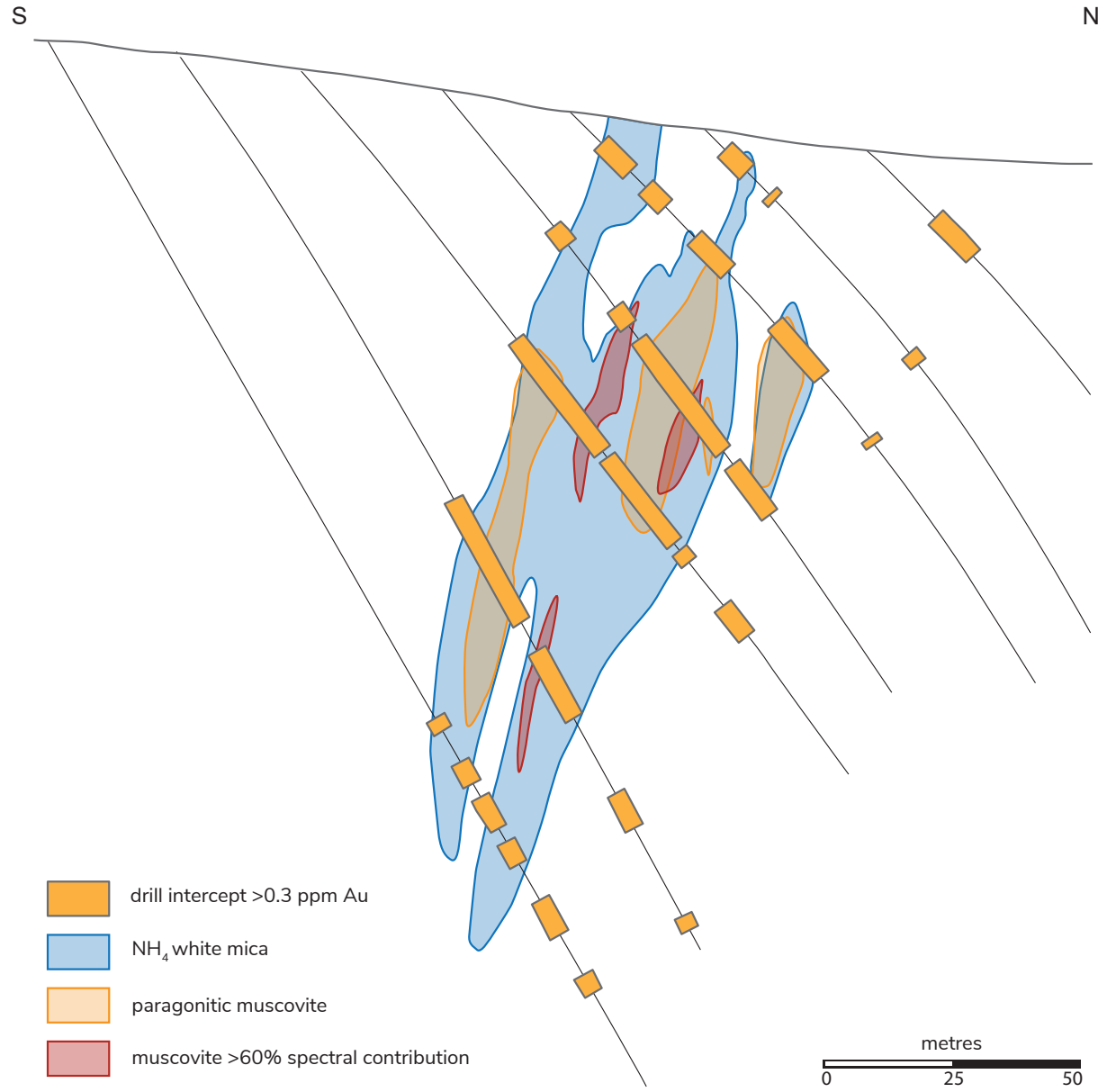


***Figure 11.*** *Cross section from the Latte zone showing concentric zoning of muscovite (with a spectral contribution >60%), paragonitic muscovite and $NH_4$ white mica surrounding Au mineralization greater than 0.3 ppm. Figure adapted from unpublished Newmont study.*

emplacement depth of ~12 km for the CCP (ibid.). MacWilliam (2018) also included ore fluid characterization that used alteration and ore mineral assemblages to bracket the fluids to ~250°C and a pH of ~5. Lead and sulphur isotope analysis completed by MacWilliam (2018) was inconclusive at determining the source of fluids and metals that formed the Coffee deposit. The lack of vertical and lateral zonation was used as evidence against a magmatic source (ibid.). Instead, the fluids were interpreted to be sourced more distally from the devolatilization of sedimentary rocks at depth (ibid.). However, MacWilliam (2018) also recognized that Coffee's characteristics are somewhat unique compared to typical orogenic deposits, and acknowledged overlap between orogenic, (reduced) intrusion-related, and Carlin-like deposit models, highlighting a need for reassessment of epizonal gold-only deposit models.

## Results

### Bedrock mapping results

The main updates to the map (Plate 1; Fig. 3) include:

- Addition of the Upper Sulphur Creek unit of orthogneiss
- Refinement of the Sulphur Creek-Snowcap contacts on the east end of the property
- Reclassification of the previous CCF as the Latte Creek damage zone (LCDZ)
- Moving the main CCF from south of the deposit to north of the deposit
- Removal of the Independence Creek fault
- Addition of Sarah's fault and the associated offset of the Supremo antiform hinge
- Addition of the gabbroic diorite intrusion west of the main deposit
- Refinement of lithology contacts in the Sugar area in the southeastern corner of the property
- Addition of an upper Snowcap assemblage psammite unit

#### *Field mapping*

Numerous mapping traverses conducted in 2022 and 2023 contributed to the updated geology map (Plate 1). The primary finding of field mapping is the definition of the Upper Sulphur Creek unit (PqSu; Plate 1) where previous maps indicated an uninterrupted panel of Snowcap schist. This unit was observed in outcrop in numerous locations and also has a remote sensing signature distinct from the surrounding Snowcap assemblage, allowing for confident extrapolation of these contacts beyond the outcrop locations (Figs. 12,13,14). This unit is demonstrated to be dextrally offset across a series of fault splays in the northern half of the property. A reconstruction of this strike-slip deformation using the Upper Sulphur Creek unit as a marker bed gives an apparent offset of approximately 25 km (Fig. 3). Within this unit, there are four locations where a stretching lineation (L-tectonite) was observed (Plate 1; Fig. 7). Additional structural mapping led to the observation of a shallow crenulation fabric in the Snowcap assemblage and also the offset of foliation across Sarah's fault (Plate 1).

Mapping across the location of the CCF as previously mapped (e.g., Ryan et al., 2013a, 2013b; Yukon Geological Survey, 2023a) demonstrated a lack of observable offset across this fault. Thus, the western ~20 km of the CCF is now shown to the north of the deposit instead of the south (Plate 1; Fig. 3). Similarly, the previously mapped Independence Creek fault is not on

the new compilation, as both the metabasalt and psammite units appear to be continuous across Independence Creek (Plate 1; Fig. 13). Field mapping was conducted iteratively with the following desktop methods in order to augment mapping in terrain with only sparse outcrops.

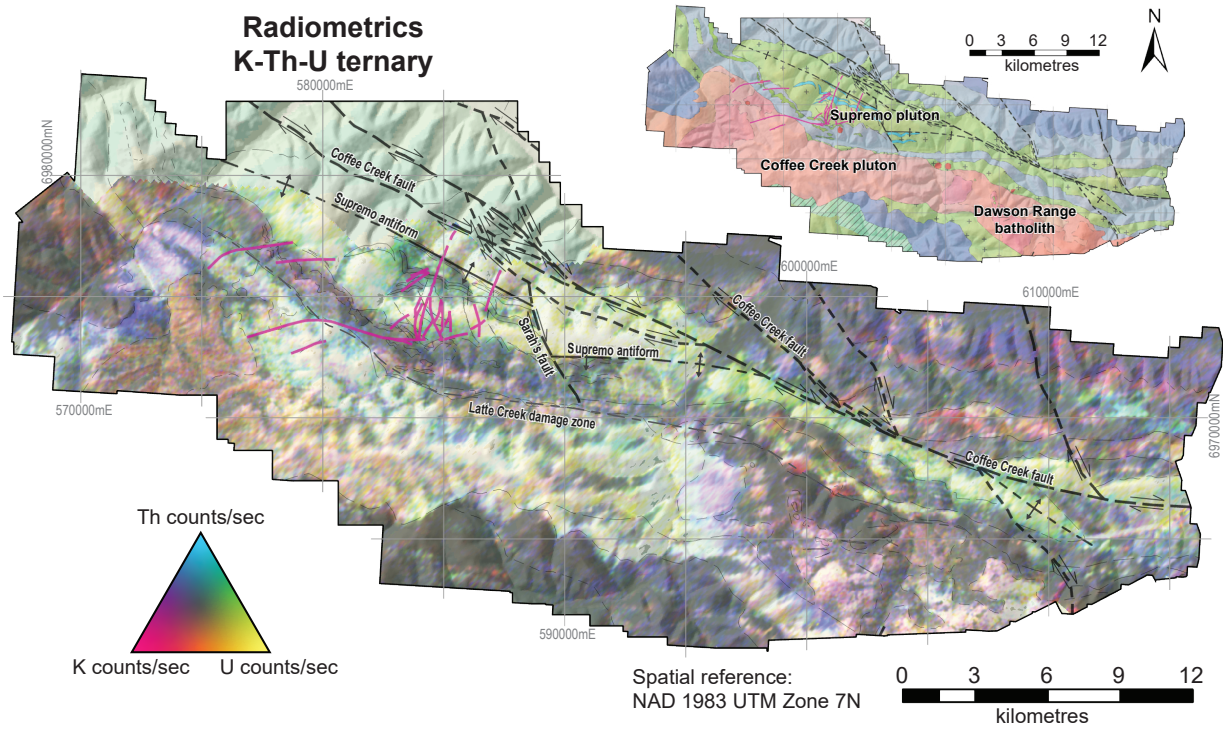


***Figure 12.*** *Airborne K-Th-U radiometrics imagery displayed with mapped contacts and structures. Dark coloured areas do not have strong radiometric signatures, bright areas contain varying abundances of Th-K-U. Inset is the property geology map used for comparing currently mapped bedrock with radiometric imagery (Plate 1; Figure 3).*

### *K-Th-U radiometrics*

All major contacts between the Sulphur Creek suite, Snowcap assemblage, and Whitehorse suite plutonic rocks are clearly observed in K-Th-U radiometric imagery (Fig. 12). Orthogneiss of the Sulphur Creek suite and the Whitehorse suite plutonic rocks display distinctive bright colours within radiometric K-Th-U ternary imagery due to the enrichment of these elements relative to the metasedimentary and metavolcanic packages of the Snowcap and Finlayson assemblages and the Klondike Schist (Fig. 12). Typically, Sulphur Creek packages are Th-enriched (green in Fig. 12), and Coffee Creek/Dawson Range plutonic rocks are K-enriched (white to pink or red in Fig. 12). Radiometric imagery was also used to differentiate intrusive phases of the CCP. In contrast to the western Coffee Creek granite, many of the eastern CCP intrusions have K-enrichment and subtle U-depletion. The radiometric data was also used to differentiate the main Supremo pluton (Sulphur Creek suite) from the Upper Sulphur Creek subunit, where the subunit is enriched in K and the main pluton is enriched in Th.

### *Soil geochemistry*

Soil factor analysis and PCA were completed on the extensive soil geochemistry dataset across the Coffee property in order to augment bedrock observations. In many cases the various element associations proved useful for differentiating felsic orthogneiss and plutonic rocks

from the surrounding metasedimentary and metavolcanic packages (Fig. 13). Soil geochemistry analysis was also effective at discerning different lithological packages within the Snowcap assemblage. The psammite subunit of the Snowcap assemblage (Fig. 6) overlying the biotite schist package can be readily differentiated by viewing black shale signatures (i.e., soil samples with Cd, Ag, Mo, Se, Zn, Pb, Cu, Hg and Bi as contributing factors; Fig. 13). A moderately high Ni-Cr-Mg-Cu-Co lithogeochemical signature highlights the main schist unit of the Snowcap assemblage (yellow and green in Fig. 13). Metabasalt lenses within the Snowcap assemblage have an even more distinct high signature of the same elements (red in Fig. 13). Similarly, the gabbroic diorite plug drilled in 2023 displays a distinct Ca, Sr, Mg, Cr, Ni and Zn geochemical signature relative to the host biotite granite (Figs. 4 and 13).

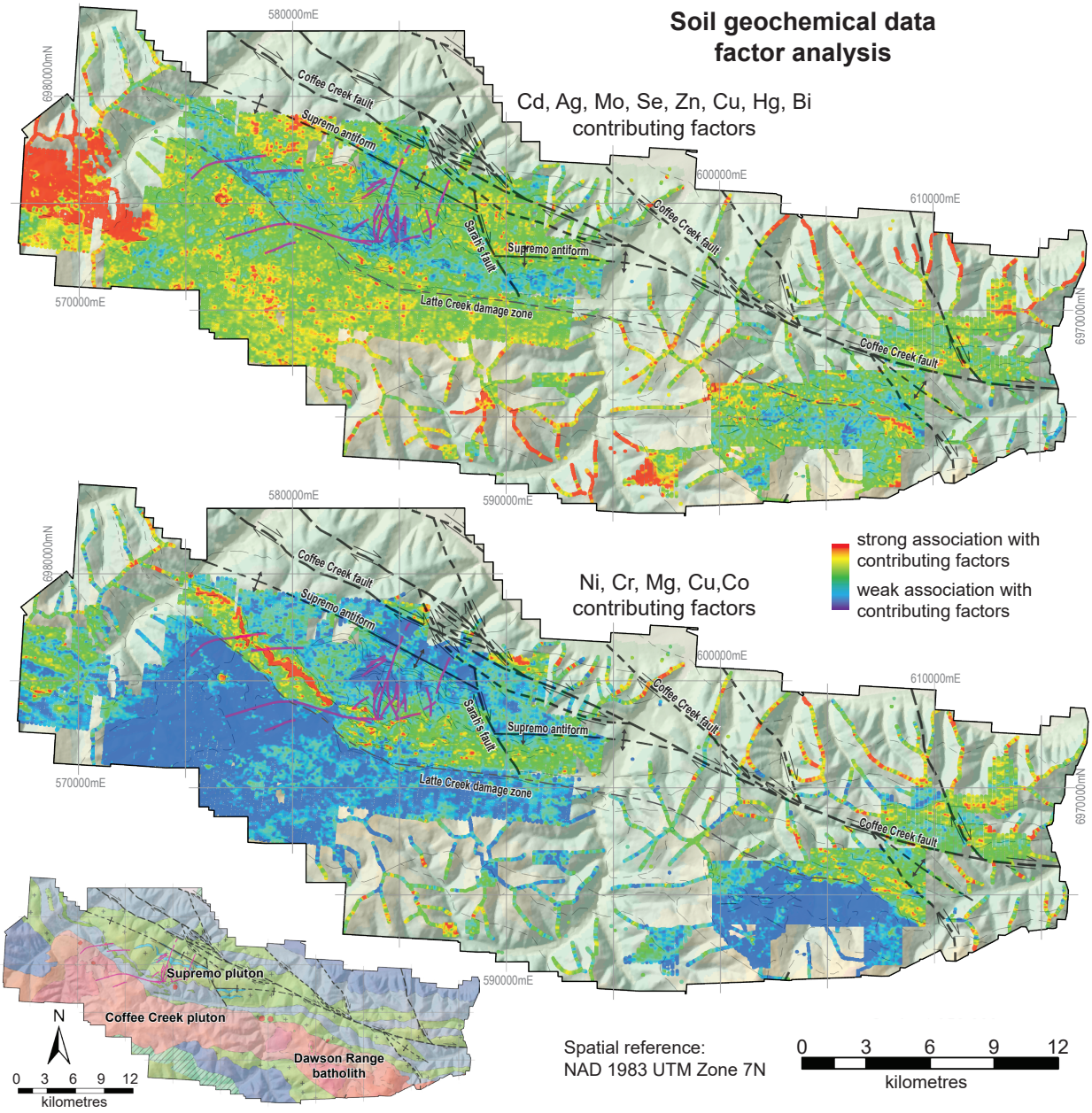


***Figure 13.*** *Soil geochemical data contoured using factor analysis. Red shades denote areas with high abundances of contributing geochemical signatures, blue shades denote areas with low abundances. Inset is the property geology map used for comparing currently mapped bedrock with soil geochemistry (Plate 1; Figure 3).*

### *Airborne and ground magnetics*

The reduction-to-pole (RTP) equal-area aeromagnetic layer (Fig. 14) is another dataset that augmented field mapping. Most notably, lenses of biotite-muscovite-feldspar-quartz schist hosted within the Supremo pluton could be extended beyond the drill-confirmed extents. The dextral offset of these mafic lenses across Sarah's fault is corroborated with this dataset (Plate 1; Fig. 14). Airborne magnetic imagery was also used in conjunction with soil geochemical data to identify potential small intrusive plugs that occur across the property. The most notable of these is the gabbroic diorite intrusion hosted within the CCP to the west of the main deposit area, which was drill tested in 2023 (Figs. 4 and 14).

### *Lidar*

The lidar dataset at the Coffee Project is high resolution (1 m) and covers the entire property. This dataset was used primarily to identify previously unrecognized fault lineaments which were later verified in the field and corroborated with the other desktop methods mentioned above (Fig. 15). Many of the inferred fault lineaments identified within the lidar imagery are coincident with apparent offsets of distinctive radiometric, geophysical and geochemical signatures (Figs. 12,13,14). The prominent northwest-trending topographic lineament to the north of the Coffee deposit (Fig. 15) was not incorporated in any previous geology map. Iterative field and desktop mapping in this area identified the Upper Sulphur Creek unit and its dextral offset across these lineaments which are now interpreted as the redefined CCF and related splays (Plate 1; Fig. 15). Bedding traces and even outcrop geomorphology can sometimes be interpreted from various lidar hillshades, thus this dataset also helped with traverse planning and lithology contact interpretations.

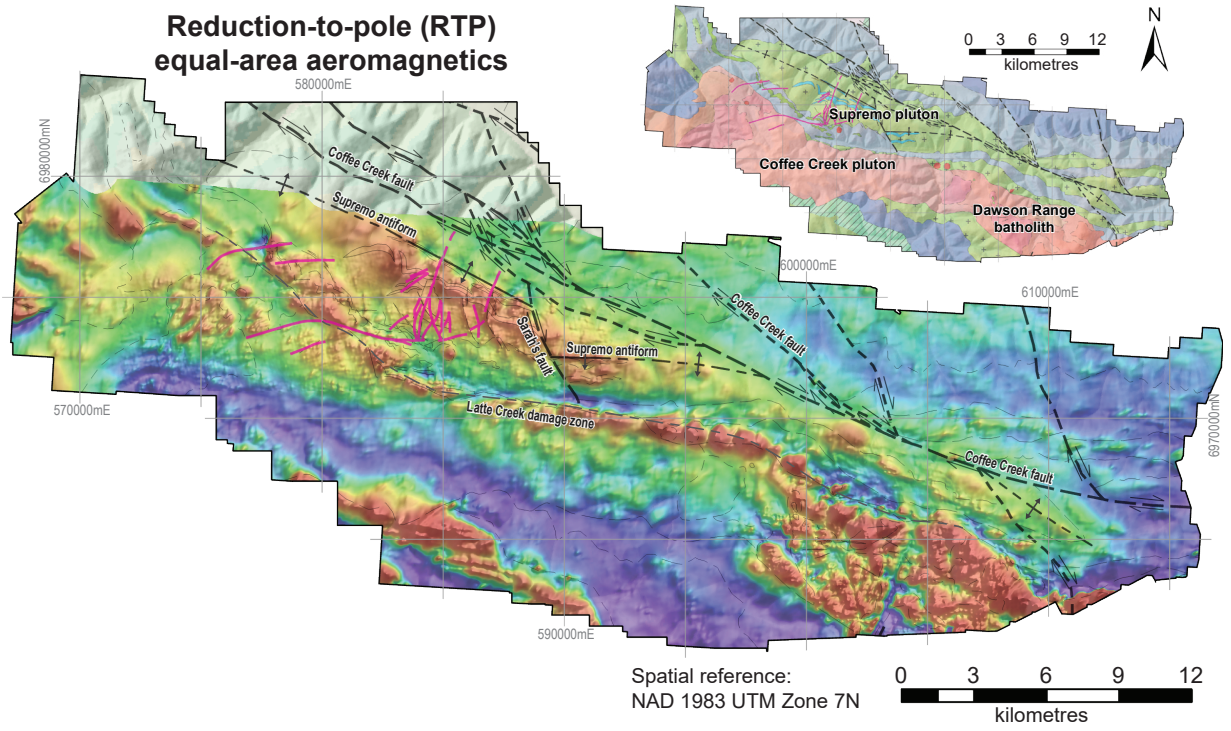


***Figure 14.*** *Airborne reduction-to-pole (RTP) equal area aeromagnetic imagery displayed with mapped contacts and structures. Conductive features are highlighted as reds and magnetic-lows are shown as blue. Inset is the property geology map used for comparing currently mapped bedrock with aeromagnetic data (Plate 1; Figure 3).*

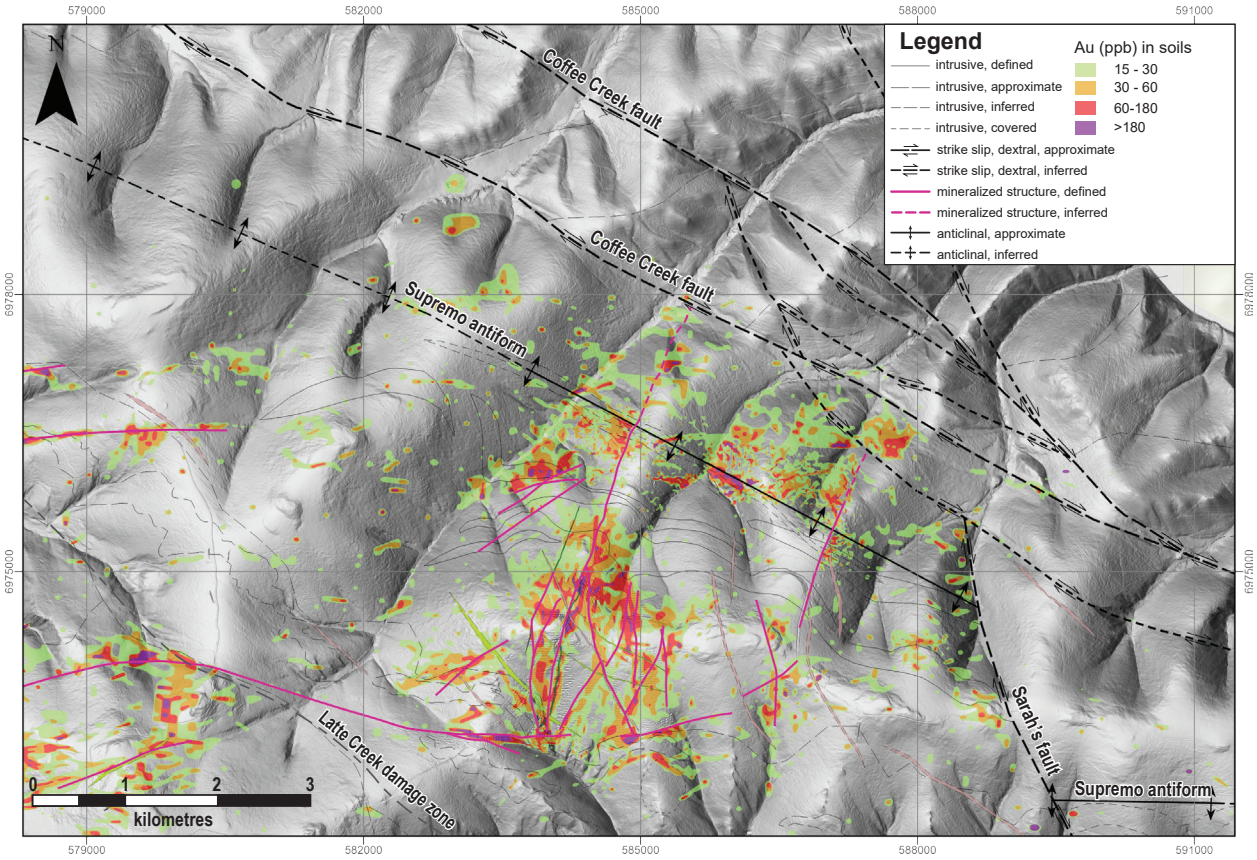


***Figure 15.*** *Light detection and range (lidar) imagery showing topographic lineaments interpreted as apparent dextral strike-slip faults. Au-in-soil geochemistry contours overlain.*

## Geochronology results

### *Zircon U-Pb results*

*Upper Sulphur Creek*

Four samples of the  Upper Sulphur Creek subunit were dated in 2022 from both the undeformed (A0666424, A0666425 and A0666426) and lineated portions (A0666427), yielding dates ranging from ~258 to ~254 Ma (Table 2 and Fig. 16).

Sample A0666424 is an undeformed granite of the Upper Sulphur Creek subunit (Fig. 3 ). It yielded euhedral to subhedral concentrically zoned zircons with aspect ratios ranging from 2:1 to 3:1 (Fig. 16). Forty-eight spot analyses yielded $^{206}Pb/^{238}U$ dates between 268 and 248 Ma, with a weighted mean age of 255.4 ± 6.3 Ma (MSWD = 1.0, n = 48).

Sample A0666425 is an undeformed granite of the Upper Sulphur Creek subunit (Fig. 3). It yielded euhedral to subhedral concentrically zoned zircons with aspect ratios ranging from 2:1 to 3:1 (Fig. 16). Thirty-seven spot analyses yielded $^{206}Pb/^{238}U$ dates between 286 and 243 Ma, with a weighted mean age of 257.2 ± 6.5 Ma (MSWD = 1.4, n = 27).

Sample A0666426 is an undeformed granite of the Upper Sulphur Creek subunit (Fig. 3). It yielded euhedral to subhedral concentrically zoned zircons with aspect ratios ranging from 1:1 to 3:1 (Fig. 16). Fifty spot analyses yielded $^{206}Pb/^{238}U$ dates between 277 and 244 Ma, with a weighted mean age of 258.2 ± 6.4 Ma (MSWD = 1.2, n = 43).

Sample A0666427 is a deformed granitic L-tectonite of the Upper Sulphur Creek subunit

(Fig. 3). It yielded euhedral to subhedral concentrically zoned zircons with aspect ratios ranging from 1:1 to 3:1 (Fig. 16). Forty-seven spot analyses yielded 206Pb/238U dates between 269 and 243 Ma, with a weighted mean age of 255.4 ± 6.4 Ma (MSWD = 1.3, n = 45).

The total range of U-Pb zircon dates obtained for the L-tectonite-bearing orthogneiss (Upper Sulphur Creek) in this study is from 264.6 to 249.1 Ma (Table 2). This overlaps with U-Pb zircon crystallization age of the main Sulphur Creek unit from MacWilliam (2018) of 263.7 ± 2.7 Ma. The similarity in ages, along with textural and geochemical similarities led to the interpretation that this previously unmapped unit is part of the Sulphur Creek suite and represents a separate intrusion with a slightly different deformation history than the main Supremo pluton.

***Table 2.*** *Zircon and apatite geochronology results from this study.*

| Sample ID | Easting | Northing | Lithology | Mineral | Method | Weighted mean age (Zrn) or York regression age (Ap) | ± Error (2σ) | Number of anlyses in calculated age | MSWD | Probability of fit (zrn) |
|---|---|---|---|---|---|---|---|---|---|---|
| A0666424 | 585182 | 6979475 | Upper Sulphur Creek suite (undeformed) | zircon | LA-ICP-MS | 255.4 | 6.3 | 48 | 1.0 | 0.41 |
| A0666425 | 589814 | 6976863 | Upper Sulphur Creek suite (undeformed) | zircon | LA-ICP-MS | 257.2 | 6.5 | 27 | 1.4 | 0.09 |
| A0666426 | 605416 | 6969705 | Upper Sulphur Creek suite (undeformed) | zircon | LA-ICP-MS | 258.2 | 6.4 | 43 | 1.2 | 0.16 |
| A0666427 | 609926 | 6969342 | Upper Sulphur Creek suite (L-tectonite) | zircon | LA-ICP-MS | 255.4 | 6.4 | 45 | 1.3 | 0.08 |
| H689002 | 584786 | 6973649 | Porphyritic diorite dike | zircon | LA-ICP-MS | 107.1 | 2.8 | 41 | 1.3 | 0.1 |
| H689002 | 584786 | 6973649 | Porphyritic diorite dike | apatite | LA-ICP-MS | 111.9 | 6.1 | 51 | 1.7 | |
| H689003 | 584173 | 6974152 | Monzogabbro dike | apatite | LA-ICP-MS | 100.0 | 6.0 | 33 | 1.0 | |
| H689009 | 584111 | 6973849 | Monzogabbro dike | apatite | LA-ICP-MS | 109.0 | 4.0 | 61 | 1.0 | |
| H689011 | 584314 | 6974200 | Porphyritic diorite dike | apatite | LA-ICP-MS | 113.1 | 5.8 | 56 | 1.3 | |

### *Cretaceous dike*

Sample H689002 is from a porphyritic diorite dike (GDIORp; Fig. 5). It yielded euhedral to subhedral concentrically zoned zircons with aspect ratios ranging from 1:1 to 3:1 (Fig. 16). Forty-five spot analyses yielded $^{206}Pb/^{238}U$ dates between 119 and 100 Ma, with a weighted mean age of 107.1 ± 2.8 Ma (MSWD = 1.3, n = 41). This age predates the age range for the CCP (~103–97 Ma; Table 2). This is consistent with geological observations and previous ages obtained for this phase, overlapping with the 106 ± 2.2 Ma date of the Yukon Geological Survey (2023b).

## *Apatite U-Pb results*

Two samples of the plagioclase-porphyritic diorite dike (GDIORp) were also sampled for U-Pb apatite dating (Table 2 and Fig. 17). Sample H689002 yielded a lower intercept date (York regression) of 111.9 ± 6.1 Ma (MSWD = 1.7), whereas sample H689011 yielded a lower intercept date (York regression) of 113.1 ± 5.8 (MSWD = 1.3). These dates overlap with the zircon age presented above (Figure 18).

The monzogabbro dike phase (GBRO) did not yield any zircon after separation. Apatite from two samples (H689003 and H689009) was analysed using U-Pb geochronology and yielded dates (York regression) of 100 ± 6 Ma (MSWD = 1) and 109 ± 4 Ma (MSWD = 1.0), respectively. The date for H689009 is older than the age of the Coffee Creek granite, which the monzogabbro dike phase crosscuts in the Kona area (Fig. 18). The date is in conflict with geological observations and therefore is not interpreted to reflect the timing of emplacement. It is possible that the apatite represent a xenocrystic population from nearby mid-Cretaceous GDIORp dikes. In contrast, sample H689003 overlaps the age of the Coffee Creek granite.

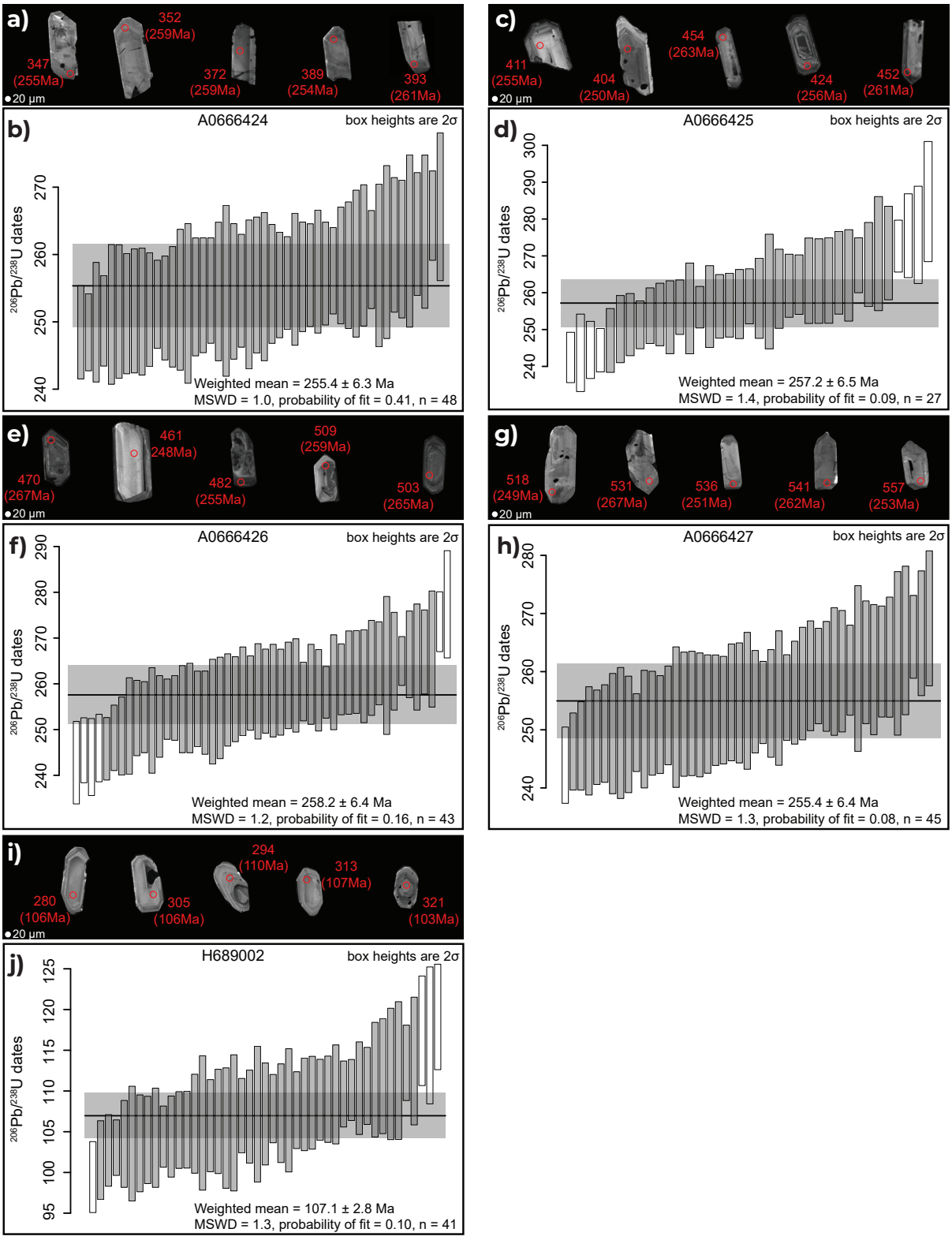


***Figure 16.*** *U-Pb zircon geochronology results from this study. (a,c,e,g,i) Cathodoluminescence images of representative zircon analyzed by LA-ICP-MS (red analysis number with $^{206}Pb/^{238}U$ date in smaller text below. (b,d,f,h,j) Ranked plot of $^{206}Pb/^{238}U$ dates determined by LA-ICP-MS. Bar heights are 2σ The horizontal grey bar represents the weighted mean age (middle of bar), and associated error of the weighted mean age (height of bar). Ages include external error of the reproducibility of reference materials.*

It is possible that the young end of the uncertainty range of apatite for H689003 represents crystallization of the GBRO dikes immediately after emplacement of the Coffee Creek granite. There is a second younger population in sample H689003 with a York regression age of 46 ± 13 Ma (MSWD = 0.5; Fig. 17). This Paleogene population may indicate a secondary pulse of mafic intrusives or a second thermal event after crystallization of the dike.

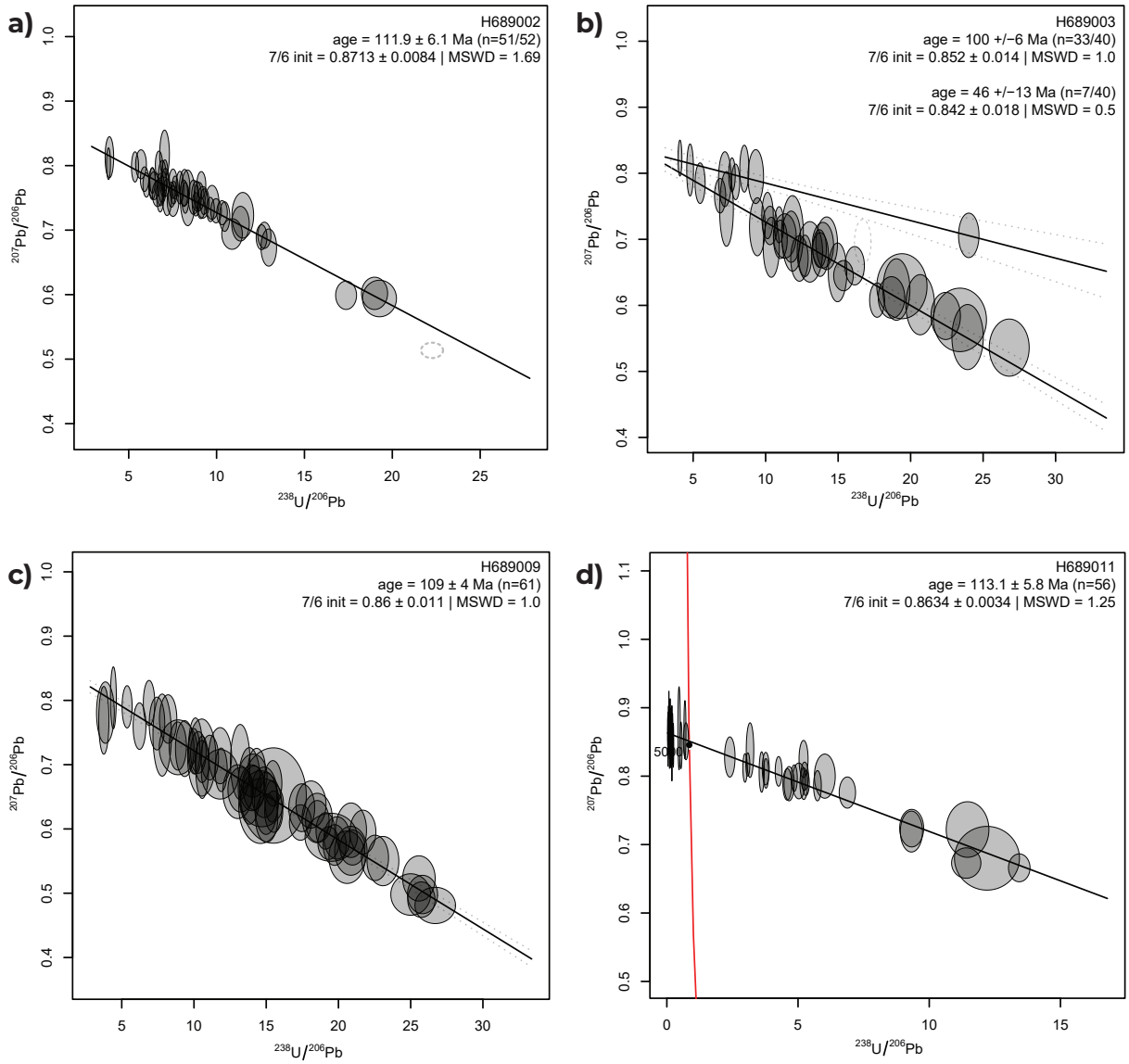


***Figure 17.*** *Apatite U-Pb geochronology results. Terra-Wasserburg concordia plots of LA-ICP-MS analyses. Ellipse radii and grey halo on regression line are 2σ. Excluded analyses in white with dashed outline.*

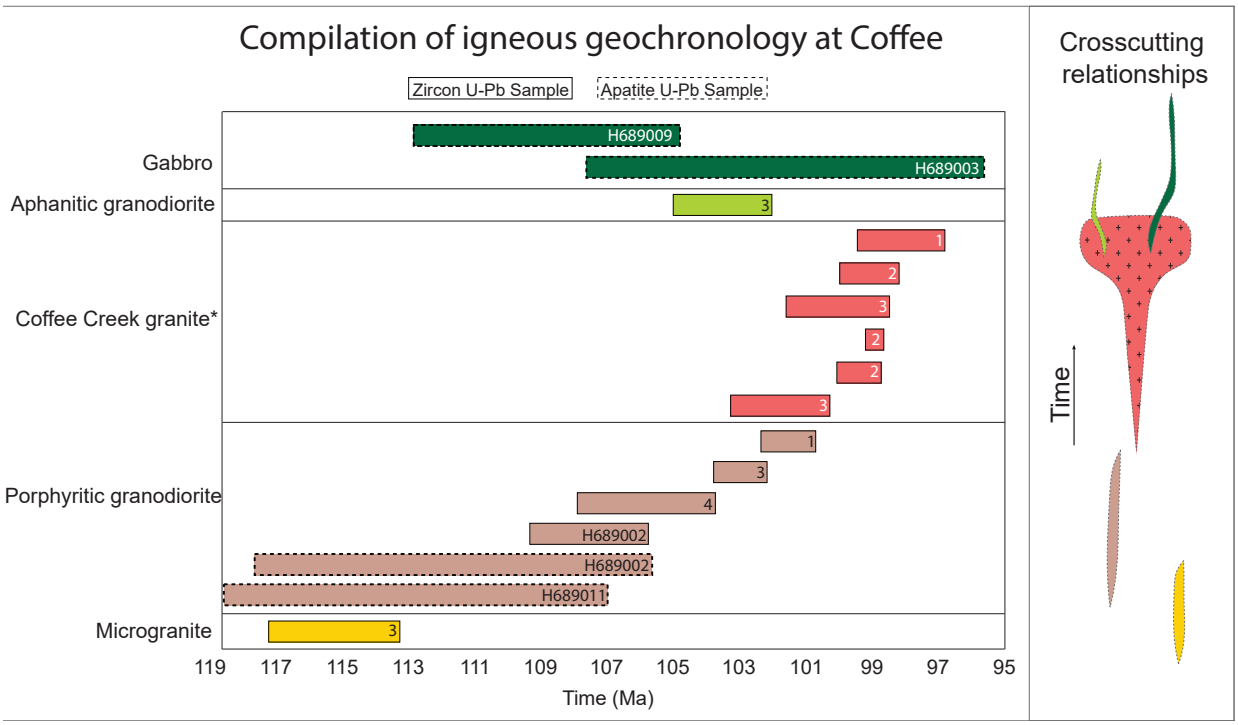


***Figure 18.*** *Diagram of compiled igneous age determinations available at Coffee. Crosscutting relationships are demonstrated by the schematic on the right. Bar widths are 2σ. Previous studies labelled by number: 1) Buitenhuis (2014) and references therein; 2) McKenzie et al. (2013); 3) MacWilliam (2018); 4) Yukon Geological Survey, 2023b. Current study sample numbers correspond to Table 2. *Including Hbl quartz monzonite.*

## Geochemistry results

A total of 21 dike samples were collected from diamond drill core at the Supremo deposit for whole-rock geochemistry. The three most prevalent dikes; aphanitic diorite (GDIORa), porphyritic diorite (GDIORp) and monzogabbro (GBRO), as well as the gabbroic diorite plug (GABD) that intrudes into the CCP (Plate 1), can be differentiated using major element, immobile element and rare-earth element (REE) plots (Fig. 19). These dikes display compositions ranging from dacitic/andesitic to basaltic on major element plots (Fig. 19a). On the Th-Co discrimination diagram (Fig. 19c), they plot as high-K/Shoshonitic intrusions. Typically the dioritic intrusions show more calcic signatures whereas the monzogabbro displays an alkali-calcic signature (Fig. 19b,d).

Two other regional igneous datasets are also plotted in Figure 19 for comparison with the Coffee dikes; the mid-Cretaceous Mount Nansen group (Klöcking et al., 2016) and Late Cretaceous Carmacks group (Johnston et al., 1996). In all plots the porphyritic granodiorite and aphanitic granodiorite dike samples plot in the mid-Cretaceous field with the Mount Nansen dataset, whereas the monzogabbro dike samples plot in the Late Cretaceous field with the shoshonitic Carmacks volcanics (Fig. 19). In immobile element plots, the gabbroic diorite plug also plots with the Late Cretaceous Carmacks/monzogabbro group (Fig. 19c,d), suggesting that the gabbroic diorite plug (GABD; Plate 1) is genetically related to the monzogabbro dikes (GBRO; Plate 1). These same groupings are evident in REE spider diagrams with the Carmacks/Coffee GBRO group having a gentler La-Eu slope than the Mount Nansen/Coffee granodiorite group (Fig. 20). Together these plots suggest that Coffee's monzogabbro dikes and gabbroic diorite plugs are Late Cretaceous in age.

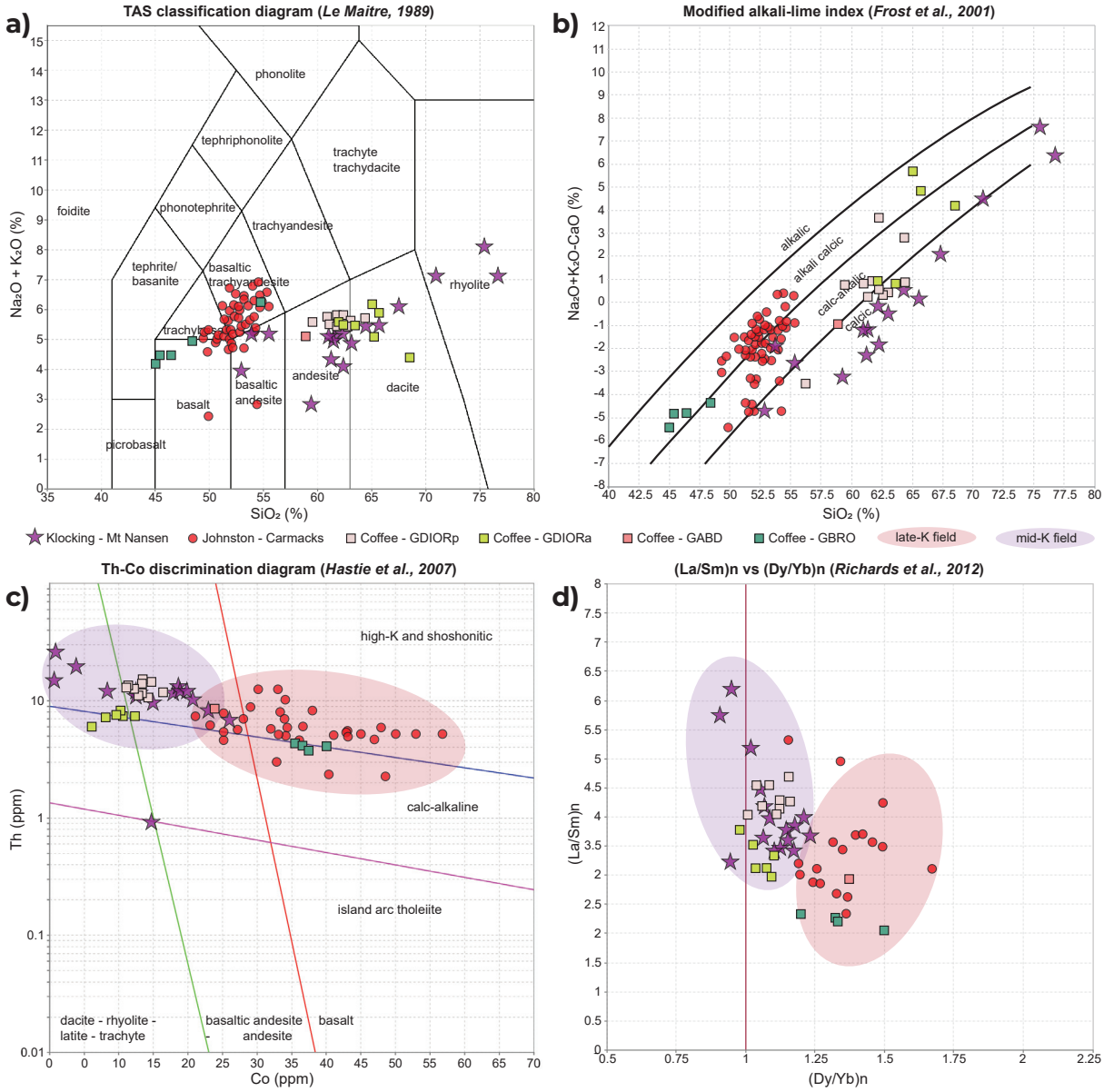


***Figure 19.*** *Geochemical differentiation plots for mid- to Late Cretaceous dikes. Coffee dike samples are plotted as squares. Red circles represent Carmacks volcanics data from Johnston et al. (1996). Mount Nansen group intrusives data from Klöcking et al. (2016) shown as purple stars.*

### *23-MAC-DD055*

Drilling in 2023 intersected atypical gold-bearing mineralization in hole 23-MAC-DD055 characterized by extensive disseminated arsenopyrite and hydrothermal breccias with mineralized arsenian pyrite clasts in close spatial proximity to banded quartz-calcite-sulphide veins (Fig. 21). These are similar textures to those described by MacKenzie et al. (2013) and may be interpreted as similar to the 'epithermal-like' textures observed by Buitenhuis et al. (2015). The primary mineralized interval in this hole has metal associations of Au-As-Sb, typical of Coffee mineralization, as well as slightly elevated Ag, Pb, Te, W, Zn and K, which are not recognized as commonly occurring metals associated with Au at Coffee.

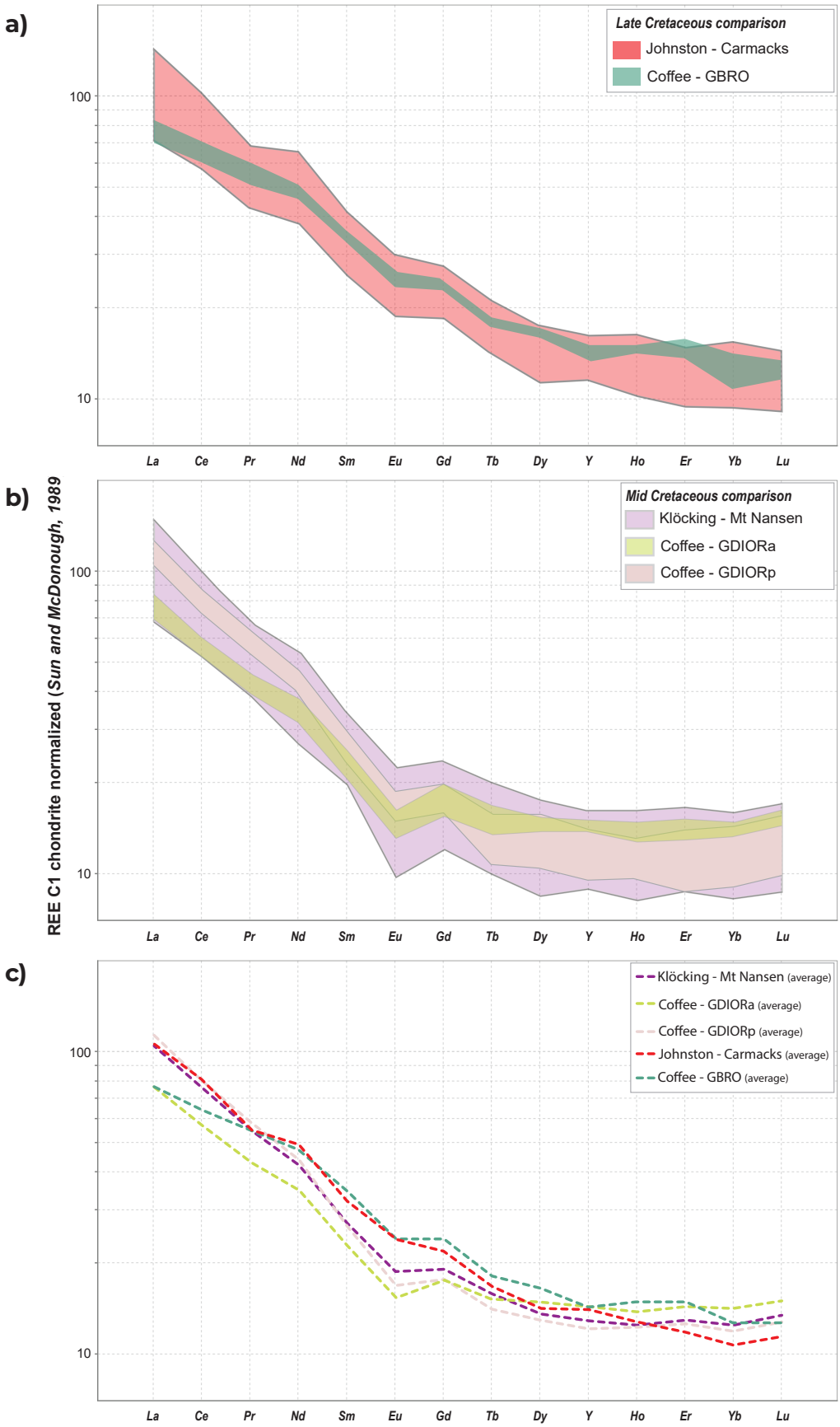


***Figure 20.*** *Rare earth element chondrite-normalized spider diagrams showing the grouping of Carmacks (Johnston et al., 1996), Nansen (Klöcking et al., 2016), and Coffee intrusions.*

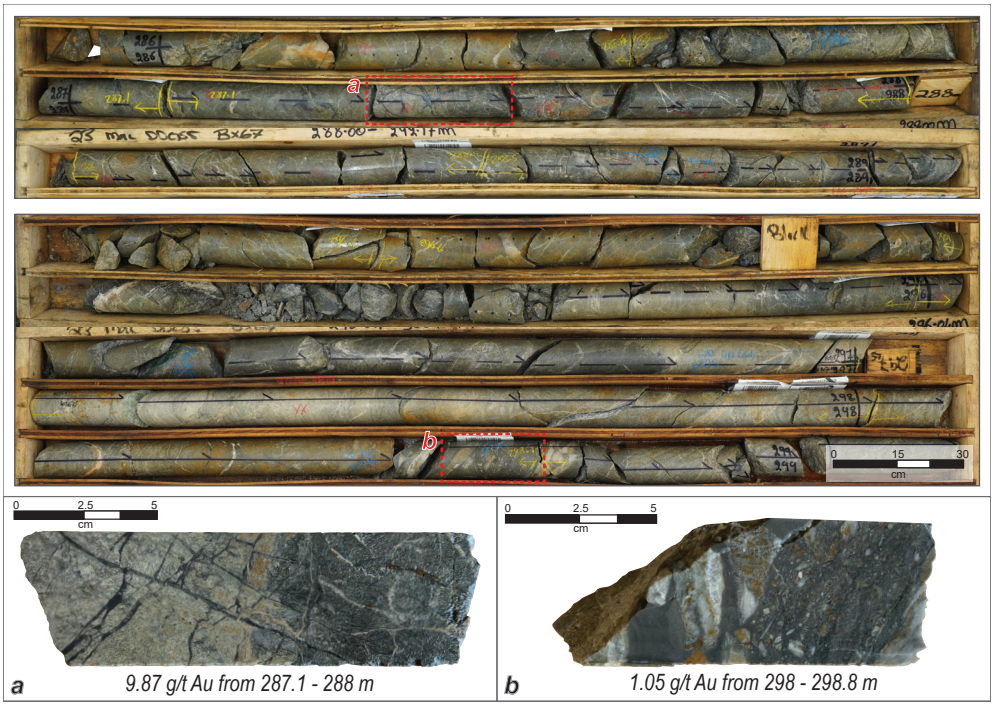


***Figure 21.*** *Drill core photos from 23-MAC-DD055 displaying textures which are atypical of Coffee-style mineralization. Insets are detailed core photos with the grade of each sample shown.* ***a)*** *Thin chalcedonic veins within strongly fractured, quartz-sericite altered orthogneiss. Sulphides are present within veins and disseminated within wallrock.* ***b)*** *Hydrothermal breccia with smokey chalcedonic matrix and angular clasts of wallrock and quartz vein material.*

## Structural analysis results

The structural analysis began with finding the magnitude and orientation of the principal stress directions required to form the fault geometries observed at Coffee (Fig. 22). The average fault plane orientations from all modelled structures in Coffee's Supremo, Latte and Double-Double zones were plotted on an equal-area lower hemisphere stereonet (Fig. 22a). Using two-plane averaging with the Stereonet software, great circles representing the two average planes of all mineralized structures at Supremo were calculated. The orientations of these two planes and the acute angle between them is consistent with the orientations of the main gold-bearing structures at Supremo: T3 and T5 (Fig. 22b) which are assumed to be conjugate structures. The maximum principal stress ($\sigma_1$) plots as the acute bisector, the minimum principal stress ($\sigma_3$) as the obtuse bisector, and the intermediate principal stress ($\sigma_2$) is calculated from these and is nearly vertical. Next, the failure envelope for unfractured orthogneiss was plotted on a Mohr diagram using constraints from laboratory measurements of the rock tensile strength of the Sulphur Creek orthogneiss (Table 3 and Fig. 22c). The two red points represent the two average fault planes shown on the stereonet in Fig. 22a. Assuming the stress shape ratio is similar to the most common ratio determined for the Earth's crust, (i.e., ~0.3; Lisle et al., 2006), the magnitude of the principal stress directions can be determined in the MohrPlotter software using Equation 1 (Bishop, 1966; Angelier, 1975). This can also be done graphically, i.e., when the Mohr circle intersects the failure envelope for unfractured orthogneiss at the location of the observed conjugate mineralized structures (Fig. 22c). Assuming the absence of pore fluid pressure, the magnitude of the determined vertical $\sigma_2$ represents the weight of the rock column.

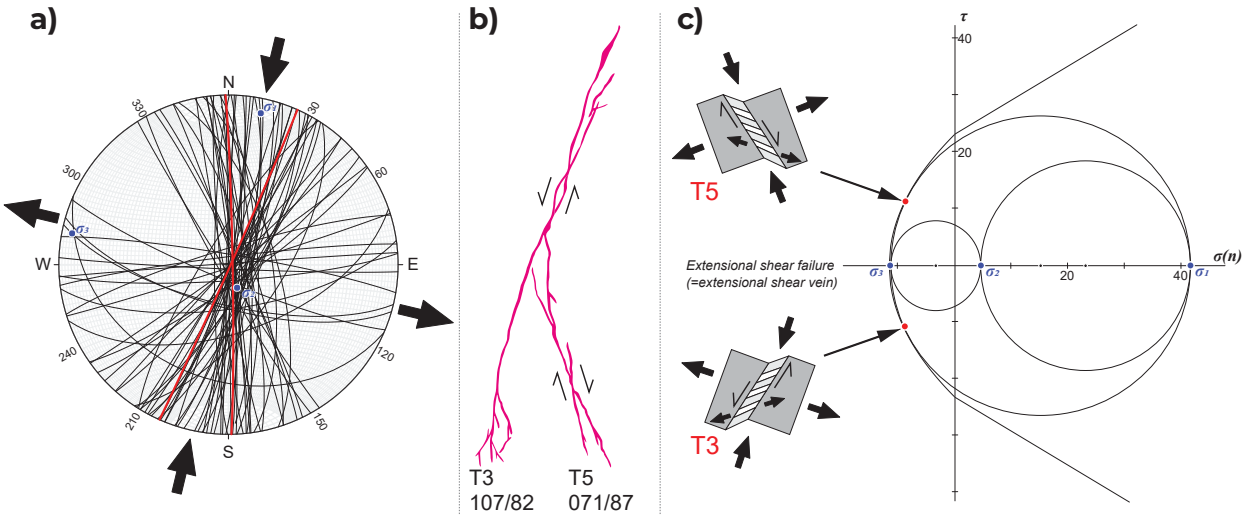


***Figure 22. a)*** *Lower hemisphere equal area stereonet with the average orientation of 3D-modelled breccia planes plotted as great circles. Red great circles indicate the two-plane averages of the ~north and ~northeast-trending structures.* ***b)*** *Schematic of Supremo T3 and T5 structures which are roughly equivalent to the average Supremo breccia planes in part a.* ***c)*** *Mohr-Coulomb diagram showing the relationship between the red planes (red dots) and the failure envelope for unfractured Sulphur Creek orthogneiss. Plots created using Stereonet and MohrPlotter software (Allmendinger, 2023).*

Equation 1: Stress Shape Ratio (Bishop, 1966; Angelier, 1975):

$$\Phi = \frac{(\sigma_2-\sigma_3)}{(\sigma_1-\sigma_3)}$$

In Figure 22a the intersection angle between the two average Supremo planes is 31°, which is less than the 60° that would be expected of typical Andersonian conjugate faults forming under compression. It indicates an oblique extensional mechanism of failure for these structures (Fig. 22c), which is compatible with mineralization emplacement along their full length. The vertical orientations of these structures and of $\sigma_2$ suggest that they formed in a strike-slip tectonic setting. The inferred kinematics is corroborated by mineral vein lineations observed in an exploration trench in the Supremo T3 structure that indicate a most recent strike-slip kinematic.

***Table 3.*** *Rock mass characteristics determined by laboratory based geotechnical studies (unpublished SRK study, 2016)*

| **Average intact rock properties** | |
|---|---|
| Lithology | Orthogneiss |
| Unconfined compressive stress | 82 Mpa |
| Indirect tensile strength | 11.6 Mpa |
| mi (analagous to the angle of friction) | 12° |

***Table 4.*** *Principal stress magnitudes from Mohr circle diagram in Figure 24.*

| **Principal stress magnitudes (MPA)** | | |
|---|---|---|
| $\sigma_1$ | $\sigma_2$ | $\sigma_3$ |
| 41.5 | 4.54 | -11.3 |

The calculated magnitude of the principal stress directions for the average Supremo planes are shown in Table 4. With a vertical $\sigma_2$ assumed to represent solely lithostatic pressure, and using an assumed pressure gradient of 25 MPa/km, the weight of the overlying rock column can be used to infer the depth at which these structures formed. Thus the 4.54 MPa calculated for $\sigma_2$ equates to a depth of just ~200 m below paleosurface. Since no pore fluid pressure is assumed, this represents an absolute minimum depth of formation of the conjugate Supremo structures.

The previously interpreted maximum depth of formation of the Coffee deposit was ~5 km (MacWilliam, 2018). To fracture the orthogneiss at this depth, a pore fluid pressure in excess of 100 MPa would be required. Near the Earth's surface pore fluid pressure is usually hydrostatic, but deeper in the crust it can exceed this level in two ways: first, plastic deformation can reduce local pore volume; second, fluid pressures can increase due to fluid production (Cox, 2020). The primary mechanism for fluid production in the crust is metamorphic dehydration, which peaks for most rocks during the transition from greenschist to amphibolite metamorphism (Gaboury, 2019). Additionally, a subsidiary source of fluids can originate from magma. Given that mineralization at Coffee occurred at least 100 million years after plastic deformation and greenschist-amphibolite metamorphism (Allan et al., 2013; MacWilliam, 2018; Colpron et al., 2022), it is unlikely that increased pore fluid pressure was a driver for mineralization at Coffee. Although some pore fluid pressure was likely present, the lack of abundant hydrothermal brecciation and associated intense quartz-carbonate vein stockworks, combined with the timing of Coffee gold mineralization, it is likely it formed in pressures far below this threshold.

# Discussion

## Structural setting

The pre-mineralization deformation of the Coffee host rocks is shown in Figure 23. The $D_1$ flattening episode that produced the penetrative planar fabric ($S_1$) observed at Coffee is inferred to peak at temperatures above 400°C and a depth probably greater than 13 km based on plastic deformation of feldspars and a nominal ~30°C/km geothermal gradient (Fig. 23a,b,c; e.g., Passchier and Trouw, 1996). Field mapping during 2022 and 2023 found that these early $D_1$ phases of deformation are overprinted by a transtensional event as seen by the L-tectonite lineation fabric within the Upper Sulphur Creek unit ($L_{2a}$; Figs. 7 and 23d). These lineations are defined by plastically deformed feldspar, quartz and micas, indicating temperature conditions >400°C (e.g., Passchier and Trouw, 1996). This represents the first and hottest phase of transtensional deformation and must have occurred prior to cooling through $^{40}Ar/^{39}Ar$ mica closure temperatures (~300–400°C) in the Jurassic (195–148 Ma; MacWilliam, 2018; Yukon Geological Survey, 2023b).

The Supremo antiform is also inferred to have formed under transtension in this timeframe by mechanisms outlined in Fossen et al. (2013) prior to regional cooling through mica $^{40}Ar/^{39}Ar$ closure temperature (Fig. 23e) and likely occurred following the formation of the Upper Sulphur Creek L-tectonite. In Figure 23e, stretching lineations would occur in the outer bounding blocks of the shear zone, which on the Coffee property would be the Upper Sulphur Creek unit (Fig. 7), whereas the folding occurs in between these blocks (Supremo antiform; Plate 1). Regionally, other evidence for this transtensional deformation occurs in the Whitehorse trough, where the sedimentary records reflect sinistral transtension during the Jurassic (van Drecht et al., 2022). This tectonic setting is compatible with the observed development of L-tectonites, and with the geometry of the Supremo fold at Coffee ($F_{2b}$; Fig. 23h; Fossen et al., 2013). In this context, the orientation of the $L_{2a}$ fabric is predicted to be parallel to the Supremo antiform

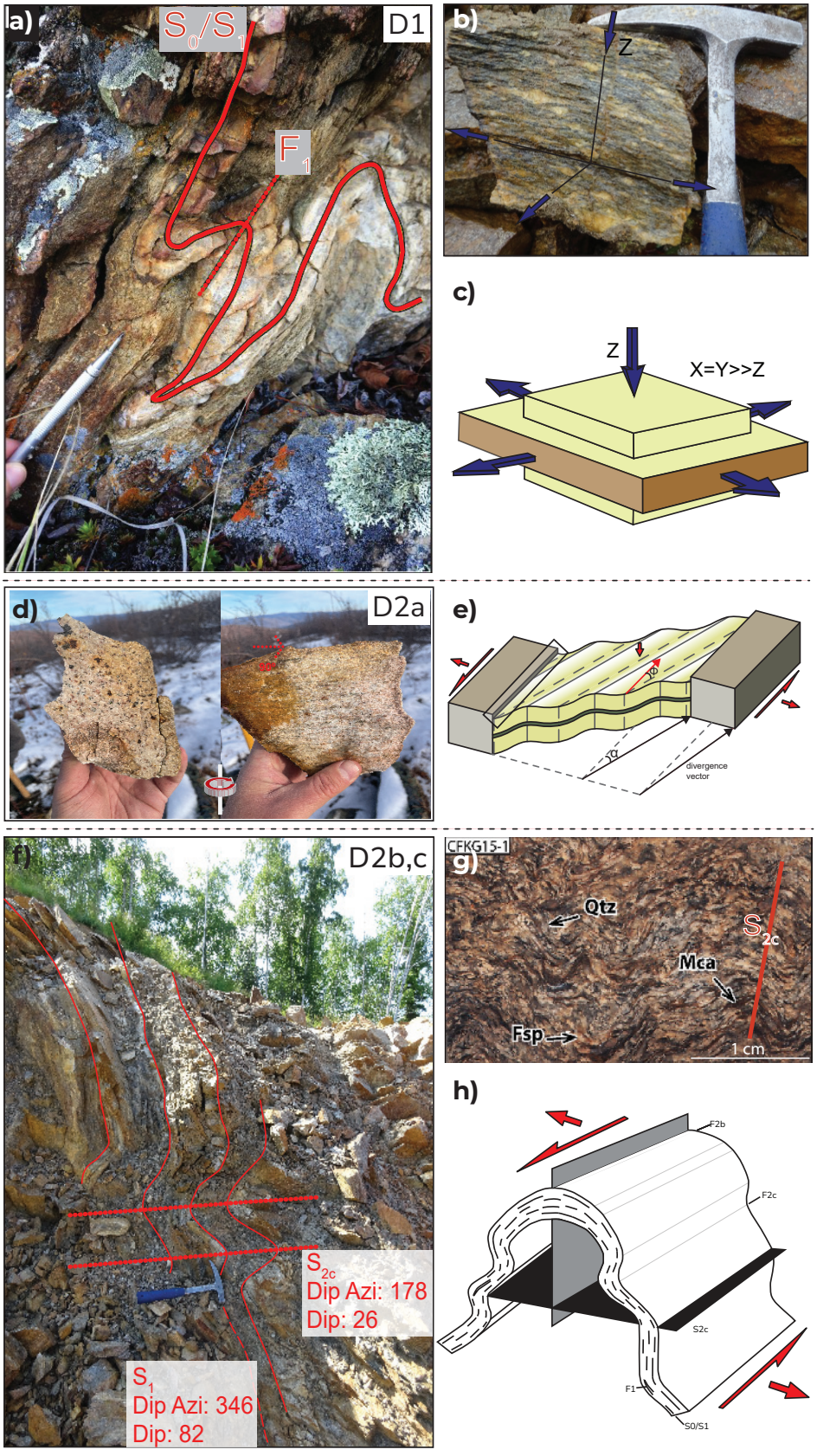


***Figure 23.*** *Pre-mineral structural deformation observed at Coffee. D1 – formation of S-tectonites and earliest isoclinal folds.* ***a)*** *$S_0$ primary bedding in the Snowcap and parallel $S_1$ foliation and $F_1$ tight isoclinal folding (MacWilliam, 2018).* ***b)*** *Flattening of minerals in the Sulphur Creek suite orthogneiss.* ***c)*** *Schematic diagram showing the formation of S-tectonites (modified from Fossen et al., 2013). D2A- L-tectonite fabric in select localities of the Upper Sulphur Creek unit.* ***d)*** *Hand sample of Upper Sulphur Creek with L-tectonite fabric.* ***e)*** *Schematic diagram demonstrating the formation of stretching lineations and associated folding that can occur during transtension (modified from Fossen et al., 2013). D2b,c - folding and crenulation observed at Coffee.* ***f)*** *Outcrop of Snowcap assemblage on the Coffee property demonstrating subvertical bedding and subhorizontal $S_{2c}$ fabric.* ***g)*** *Hand sample photograph of Snowcap assemblage schist demonstrating $S_{2c}$ crenulation fabric (red line) modified from MacWilliam (2018).* ***h)*** *Schematic diagram demonstrating larger-scale open folding that may form from continued transtension and its relationship to shallow crenulation fabrics (modified from Fossen et al., 2013).*

fold axis, (i.e., shallowly plunging and northwest to southeast trending). However, no oriented samples were taken of the L-tectonite during mapping. This transtensional folding mechanism is also supported by the near-horizontal crenulation fabric observed in a folded road outcrop ($S_{2c}$; Fig. 23f,g).

The metamorphic rocks, primary bedding ($S_0$) transposed into the metamorphic fabric ($S_1$), and the $F_1$ and $F_2$ folds described above, as well as the undeformed CCP, are crosscut by a network of north, northeast and east-trending faults and fault-related fractures ($D_3$). The most significant of these structures is the CCF system which has approximately 25 km of apparent dextral offset of bedrock units (Fig. 3). North-northwest-trending structures are also observed on the Coffee property, the most prominent being Sarah's fault which juxtaposes the northern limb of the Supremo antiform next to the southern limb (Fig. 3). Sarah's fault is inferred to be older than the mid-Cretaceous CCP, with a probable maximum age of Early Jurassic as it does not offset the granite contact but does offset the Early Jurassic Supremo antiform and the Paleozoic metamorphic rocks of the YTT.

## Fault updates

### *Coffee Creek fault*

Prior to 2023 the western end (~20 km length) of the CCF was mapped to the south of the main Coffee deposit based on a magnetic-low lineament observed in airborne geophysics (Yukon Geological Survey, 2023a; M. Colpron, pers. comm., 2024), and was interpreted as an orogen-parallel fault first activated pre-mid-Cretaceous during ~northeast-directed shortening and later reactivated during mid-Cretaceous ~north-directed shortening along the northern CCP contact (MacWilliam, 2018). Mapping transects across this lineament (Plate 1; Fig. 15) during 2022 and 2023 refined the Snowcap-Sulphur Creek-CCP contacts and demonstrated that there was no observable offset of units or the CCP contact across it at the deposit scale or any significant topographic lineaments, and thus the western ~20 km was removed from the map as a fault. Additionally, low temperature thermochronology dates, as determined by MacWilliam (2018), on either side of this magnetic lineament are very similar, suggesting that no significant vertical offset has occurred across it after cooling through the $^{40}Ar/^{39}Ar$ closure temperature range (Plate 1).

The eastern extent of the CCF has been traced in aeromagnetic datasets to meet the BCF ~18 km east of the Coffee property (Yukon Geological Survey, 2023a; M. Colpron, pers. comm., 2024). The previous interpretation of the relationship between the CCF and BCF based on these aeromagnetic lineaments was that the CCF was truncated by and potentially dextrally offset by the BCF (MacWilliam, 2018; Yukon Geological Survey, 2023a; M. Colpron, pers. comm., 2024). Geological constraints on this relationship are lacking, and the aeromagnetic data may be interpreted as demonstrating that the CCF splays off the BCF at their intersection, rather than terminating against it. Although the western ~20 km of the CCF near the Coffee deposit has been changed based on recent field mapping, as described above, the district scale trace of the CCF remains unchanged (Fig. 3; Plate 1). At the regional scale, the CCF and BCF systems appear to have similarities that may suggest a genetic relationship. The ~25 km of demonstrable offset on the CCF is similar to estimates of minimum geologically demonstrable offset on the BCF system (Johnston, 1999). Additionally, like much of the BCF fault system, the CCF system is adjacent to mid-Cretaceous plutons (CCP and DRB; Figs. 3 and 4). The BCF system is suggested to have a control on the emplacement of Whitehorse suite plutonic rocks such as the DRB (Johnston, 1999) and in the Mount Freegold district (Friend, 2022). Sánchez et al. (2014) suggest that the Coffee gold system is also structurally related to the BCF. In

the Mount Freegold district, Friend et al. (2018) suggests the BCF may have facilitated the emplacement of Whitehorse suite intrusions, and demonstrated Late Cretaceous movement on the BCF, outlining a potentially protracted fault-intrusion relationship from mid- to Late Cretaceous. At a regional scale, it is possible the CCF plays a similar role for the CCP near Coffee, but as discussed above direct deposit-scale evidence of this relationship is lacking as there is no direct interaction between the fault and pluton observed, only a magnetic low and brecciation near the northern CCP contact. Another possibility is that following the intrusion of the DRB and CCP there was sufficient rheological contrast between the batholith and the surrounding YTT that regional stresses were focused near the contact, creating the present-day spatial pattern of the BCF-CCF system that approximately follows the curved northeastern contact of the DRB and CCP (Fig. 24).

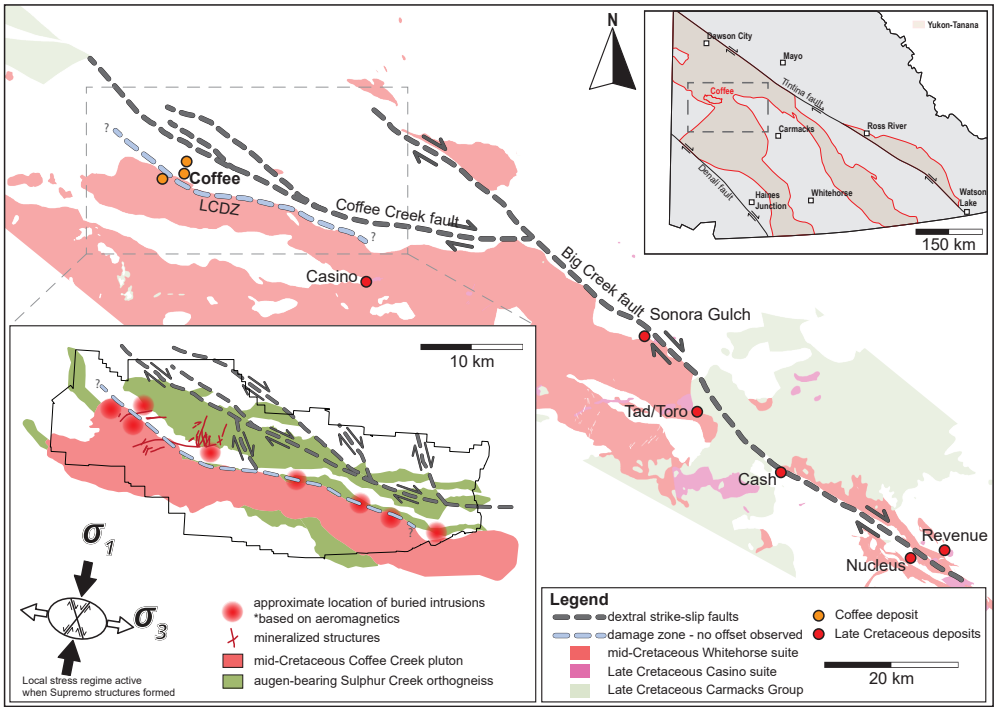


***Figure 24.*** *Overview map of the spatial relationship between the Coffee Creek fault (CCF) and the Big Creek fault (BCF) with Late Cretaceous mineral deposits represented as red dots, and the main Coffee mineralized zones represented by orange dots. The large inset map in the lower left corner shows the interpreted orientation and direction of movement along the CCF system, approximate locations of unexposed mafic intrusions interpreted from magnetic anomalies (red circles), and the interpreted stress regime for oblique-extensional faulting at Supremo.*

### *Latte Creek damage zone*

The DRB intrudes along a major terrane boundary between YTT rocks to the northeast and ancestral North American-affinity rocks in the southwest (e.g., Ryan et al., 2013a, 2013b; MacWilliam, 2018). There is no major lithology change on either side of the CCP ; however, it is possible that it intruded along a lesser splay of this terrane-bounding fault system which is now obscured by the intrusive body of the CCP itself. The northern CCP contact is known to be brecciated where it has been intersected in drilling in the Kona North and Forte West zones (Plate 1); however, these intercepts are also coincident with mineralized east northeast-trending breccia zones (approximately ~45° oblique to the CCP contact; Fig. 4) and thus it is unclear to what extent the granite contact is brecciated outside of these zones. It is possible this brecciation is more extensive and that it represents a poorly developed fault and damage zone, despite the lack of demonstrable offset of bedrock units.

Several circular magnetic high anomalies occur along or proximal to the northern CCP contact (Fig. 15). One of these anomalies was drilled in 2023 and was found to be a gabbroic diorite intrusion (GABD; Figs. 3 and 4; Plate 1). The other untested magnetic anomalies are interpreted as similar unexposed gabbroic diorite intrusions (Plate 1). The existence of these intrusions along the northern CCP contact, coincident with the location of the formerly mapped CCF, is potentially further evidence that there is a structural corridor along the contact allowing for local dilation, despite the lack of bedrock offset. The magnetic low anomaly along the northern CCP contact in the vicinity of the Coffee deposit is instead interpreted as a poorly developed damage zone herein called the Latte Creek damage zone (LCDZ), rather than a fully developed fault.

### *Independence Creek fault*

The Independence Creek fault was also reinterpreted after 2022 field mapping and removed from the geology map as a fault for the same reason as the CCF above — there is no observable offset of bedrock units despite the lineament interpretation in some datasets (e.g., Sánchez et al., 2014). The metabasalt (PDmb; Plate 1) has unique soil geochemical signatures (Fig. 14) and acts as a marker unit. This signature is observed to cross Independence Creek with no obvious disruption (Plate 1). This unit was also observed in outcrop on the west side of Independence Creek during field mapping in 2022, likely representing an upper band of the metabasalt, similar to that observed south of the Latte zone (Figs. 3 and 4; Plate 1). Whereas it is still possible that unrecognized vertical offset may exist considering the lack of outcrop in this area, this metabasalt marker bed interpretation serves as the most direct line of evidence for a lack of offset across Independence Creek.

## Timing of mineralization

Timing constraints of Coffee gold mineralization cited in MacWilliam (2018) include: syn-mineral sericite and fuchsite $^{40}Ar/^{39}Ar$ dates (~97-93 Ma), a maximum age of mineralization based on the ~99 Ma CCP crystallization age, and a minimum age bracketed by the emplacement of the post-mineral Rhyolite Creek volcanics near the Coffee property (~57 Ma; Ryan et al., 2013a, 2013b; MacWilliam, 2018;). Mineral occurrences near Coffee including the Boulevard, Toni Tiger, and Sugar prospects, yield equivalent 97–93 Ma dates (Toni Tiger $^{187}Re/^{187}Os$ molybdenite date 95.0 ± 0.4 Ma; MacKenzie et al., 2013), so it is assumed that the $^{40}Ar/^{39}Ar$ sericite dates from MacWilliam (2018) may reflect a mid-Cretaceous hydrothermal event in the Dawson range. However, this does not explicitly rule out the possibility that Coffee mineralization is younger than this event. MacWilliam (2018) presented six $^{40}Ar/^{39}Ar$ age spectra of interpreted ore-stage sericite and fuchsite from three samples in the Latte zone. Three of the age spectra (CFD560-167.7m_1, CFD560-167.7m_2, and CFD560-167.4m) have plateaus of ~91–100% Ar released (MacWilliam, 2018), indicating that in these samples the system was either undisturbed since ~96 Ma or completely reset at that time. Another three syn-mineralization mica analyses have disturbed $^{40}Ar/^{39}Ar$ age spectra with evidence of argon loss (CFD164-454.5m_2 and CFD164-365m ), or excess $^{40}Ar$ (CFD164-454.5_1). The nonuniform ‘staircase’ pattern of the age spectra in the samples with argon loss likely reflects disturbance of the hydrothermal system after the time of the plateau date (e.g., Harrison and Zeitler, 2005). Temperature ranges for mineralizing fluids at Coffee are constrained to ~220–250°C based on alteration and sulphide mineral assemblages (Buitenhuis, 2014; MacWilliam, 2018). These low-temperature fluids may not be able to fully reset the $^{40}Ar/^{39}Ar$ chronometer system (nominal closure temperatures ~300–400°C; e.g., Harrison and Zeitler, 2005), however

some spectra presented by MacWilliam (2018) support the hypothesis that the system was disturbed at some point after the plateau date. Further work to evaluate whether $^{40}Ar/^{39}Ar$ dates were affected by later ~220–250°C ore fluids may require specific details such as the precise duration and potential temperature fluctuations of ore fluid pulses. Additionally, it is possible that mid-Cretaceous $^{40}Ar/^{39}Ar$ dates may simply reflect cooling after crystallization of the CCP and related minor hydrothermal activity.

Indirect age constraints on the timing of Coffee mineralization include mineralized intrusive phases such as the mid-Cretaceous CCP and crosscutting dikes. The geochemical grouping of Coffee granodiorite dikes with the mid-Cretaceous Mount Nansen suite dikes (Fig. 19) is corroborated by the ~107 Ma zircon date obtained for this unit in this study and is the same as existing age constraints for this unit elsewhere in the region (~106–101 Ma; Table 1; Buitenhuis, 2014; Yukon Geological Survey, 2023b). Due to the close geochemical grouping of the Carmacks volcanics and Coffee monzogabbro and gabbroic diorite, these units are interpreted to all be of a similar age, nominally ~70 Ma. However, texturally the Coffee monzogabbro and gabbroic diorite appear to be hypabyssal, not volcanic, and thus the Late Cretaceous Prospector Mountain suite, or Carmacks volcanic feeder intrusions, may be a more appropriate comparison, implying a possible age range of ~72–67 Ma (e.g., Allan et al., 2013). This Late Cretaceous inferred age is significant as the monzogabbro intrusions are most closely spatially related to mineralization, often occurring within or parallel to the Supremo T3 structure. Additional evidence for late intrusive and/or thermal event at Coffee is indicated by the secondary apatite U-Pb date population in H689003 (Fig. 17). This Paleogene signature has not been observed in other datasets at Coffee but warrants more follow-up.

Additionally, the newly mapped northern location of the main CCF system appears to truncate Au-in-soil anomalies north of the Supremo deposit, suggesting that at least the most recent movement on this fault occurred post-mineralization (Fig. 15). This would imply that there may be more Coffee-equivalent mineralization on the north side of this fault, now dextrally offset up to ~25 km; however, this has not been observed and, therefore, it may simply be that the fault bounds mineralization rather than crosscutting and offsetting it. The CCF meets the BCF to the east of the Coffee property, where its precise relationship with the BCF is unclear, but broad similarities suggest these faults may be related (see above). Recent work by Mottram et al. (2020) demonstrates two known phases of slip on the BCF system, at approximately 73 Ma and between 60–57 Ma, based on dating of fault gouge minerals and calcite veins. This demonstrates that the potentially linked BCF-CCF system was active in the interpreted timeframe of mineralization.

## Depth of mineralization

MacWilliam (2018) reasoned a maximum depth of deposit formation of ~5 km based on inferred epizonal characteristics described by previous authors (Allan et al., 2013, MacKenzie et al., 2014). Additionally, MacWilliam (2018) used the inferred ~12 km emplacement depth of the CCP based on DRB Al-in-hornblende geobarometry (McCausland et al., 2006), hydrothermal sericite and fuchsite cooling ages of ~97 to 93 Ma, and a presumed depth of ore formation of ~5 km to infer rapid exhumation rates of 2.0 to 3.5 km/myr. The Al-in-Hbl barometry used to determine pluton emplacement depth (McCausland et al., 2006) is considered an unreliable technique for shallow intrusions (Hollister et al., 1987). Thus, the ~12 km emplacement depth for the CCP may be a significant overestimation. The depth of emplacement of the CCP has large-scale implications for regional exhumation rates in the Dawson Range.

Structural analysis of Coffee's Supremo faults in this study builds upon previous estimates of relatively shallow deposit formation, bracketed at ~5 km maximum depth (MacWilliam, 2018) and ~200 m minimum depth (Fig. 22). Since the minimum depth was derived assuming no pore fluid pressure, a more realistic depth estimate of ~1 to 3 km is interpreted for the formation of the Supremo structures and gold deposition, assuming that some degree of pore fluid pressure was present (> 0 MPa and << 100 MPa). The shallow depth of deposit formation is also supported by two other geological observations in proximity to the Coffee property, assuming a Late Cretaceous age of deposit formation: 1) the Casino porphyry is presumed to have formed at typical Cu-Au porphyry depths of ~2 to 3 km, and mineralization at the Casino deposit is dated at ~74 Ma (Selby and Creaser, 2001). Furthermore, explosive breccia facies are present at Casino, attesting to its shallow level of formation (Casselman and Brown, 2017). Since there is no observed fault offset between Coffee and Casino, it is a reasonable assumption that the Coffee deposit was at a similar paleodepth at ~74 Ma; 2) Similarly, ~70 Ma Carmacks volcanics and ~57 Ma Rhyolite Creek volcanics are outcropping south of the Coffee property without any fault offset mapped (Yukon Geological Survey, 2023a, 2023b), implying that the Coffee area was at a similar near-surface paleodepth by the Late Cretaceous.

## Mineralization styles

Extensive post-mineralization oxidation and faulting at Coffee has obscured primary sulphide mineral textures over most of the deposit. Although drilling at Coffee has focused on near-surface oxide ore, hypogene sulphide ore is observed both below and adjacent to supergene oxide mineralized zones, both as disseminated wallrock replacement of biotite and Fe-phengite, and as sulphide matrix breccias and fault zones (Wainwright et al., 2011; MacKenzie et al., 2013; Buitenhuis, 2014; MacWilliam, 2018). The majority of fault-hosted primary hypogene mineralization at Coffee is within tectonic fault breccias, fault gouge and cataclasites (e.g., MacWilliam, 2018). Gold-bearing quartz-carbonate vein stockwork zones are rarely observed and are volumetrically minor.

Mineralization observed in 23-MAC-DD055 contained slightly elevated Ag, Pb, Te, W, Zn and K; a metal association that is atypical of the bulk of Coffee mineralization. This signature is recognized sporadically elsewhere in the deposit and is not exclusively related to quartz-carbonate rich or potentially 'epithermal-like' intervals. Previously, Coffee was described to have a strictly Au-As-Sb metal association, with no recognized zoning, which was used as an argument against a potential magmatic point-source of heat and mineralizing fluids (MacWilliam, 2018). The extent of the subtle Au-As-Sb ± Ag-Pb-Te-W-Zn-K metal signature is not fully understood currently due to the uneven distribution of four-acid digestion geochemistry on the project. The recognition of this metal signature here may imply a previously unrecognized magmatic component to Coffee mineralization, although many of these elements are also present and associated with gold in orogenic (e.g., Groves et al., 2020) and Carlin-type (e.g., Muntean et al., 2011) systems. The occurrence of gold-bearing quartz-carbonate interval in 23-MAC-DD055 is approximately 3 km north of the Double-Double and Latte zones where gold-bearing epithermal-like textures were observed previously (MacKenzie et al., 2013; Buitenhuis, 2014).

The significance of the potentially epithermal-like mineralized intervals observed by MacKenzie et al. (2013), Buitenhuis et al. (2015), and that observed in 23-MAC-DD055 (Fig. 21) is not yet understood. It is possible that it represents rare preservation of the primary ore textures at Coffee (i.e., pre-tectonic brecciation and oxidation), an overprinting event or latest phase of an evolving mineralizing fluid (Buitenhuis et al., 2015), or it may be unrelated to the main

volumetrically significant mineralizing phase. Considering a probably later and shallower mineralization setting suggested above, together with the presence of potentially epithermal-like mineralization, a reconsideration of the overall mineral system model at Coffee is warranted.

## Potential fluid sources

The 'deep later' model of Stüwe et al. (1993) quoted by MacWilliam (2018) presents a reasonable hypothesis of how metamorphic fluids may be responsible for Coffee mineralization in the proposed post-orogenic timeframe of ~96 Ma. Staples et al. (2016) outline Early to mid-Cretaceous (~146–118 Ma) metamorphism in the Australia Mountain domain which was interpreted to underly Coffee host rocks at that time, followed by mid-Cretaceous exhumation ca. 112 Ma. This scenario outlines a time window of approximately 22 Ma (118–96 Ma) for metamorphic fluids to travel from the Australia Mountain domain to the site of mineralization in the Coffee host rocks, which is within the timeframes outlined by Stüwe et al. (1993). The nearby Boulevard and Longline occurrences are evidence of mid-Cretaceous fluid activity in the region and are interpreted as orogenic in origin by some authors (Joyce, 2002; Allan et al., 2013; McKenzie et al., 2013). However, this hypothesis becomes a less plausible model for the Coffee deposit when the evidence of a later (Late Cretaceous) window of mineralization is considered, since it is significantly farther removed in time from the metamorphism providing the fluids. MacWilliam (2018) also investigated Pb, S, O and C isotopes to identify the fluid source but the results were inconclusive. MacWilliam (2018) found Coffee S isotope values range from -3 to 7‰, which may be consistent with either mantle or magmatic sources. The apparent lack of deposit-scale metal and alteration zonation led MacWilliam (2018) to rule out the CCP as a potential fluid source.

The gabbroic diorite intrusion drilled in 2023 (GABD; Plate 1) and the numerous inferred intrusions near the northern CCP contact present a newly discovered potential non-metamorphic fluid source for Coffee mineralization. Geochemical similarities between the gabbroic diorite intrusion drilled in 2023 (GABD; Plate 1), monzogabbro dikes (GBRO; Plate 1), and Carmacks volcanics (Fig. 20), suggest that these are likely geochemically related rocks although no dating has yet been conducted on these intrusions (Fig. 24). Other Late Cretaceous intrusions along trend of Coffee adjacent to the BCF system (e.g., Casino, Nucleus and Revenue) have been linked to coincident slip phases on this fault, outlined by field relationships and supported by fault gouge mineral dating (Mottram et al., 2020; Friend, 2022). There appears to be a similar spatial correlation between the unexposed intrusions at Coffee and the LCDZ along the CCP contact (Fig. 24).

## Geological model

A reconstruction of the regional setting prior to and during mineralization is outlined in Figure 25. Early metamorphic fabrics were formed during Jurassic orogenesis under a dominantly northeast shortening direction (Colpron et al., 2022). The L-tectonite fabric observed in the Upper Sulphur Creek unit indicates an early phase of transtension prior to the Middle Jurassic cooling through mica $^{40}Ar/^{39}Ar$ closure temperatures ($T_0$). This stress regime may also account for shallow $S_{2c}$ foliation and the formation of the $F_{2b}$ Supremo antiform (Fig. 23).

These early ductile fabrics were then crosscut by northwest-trending faults such as Sarah's fault at $T_1$ prior to intrusion of the CCP in the mid-Cretaceous. This phase of faulting may be coincident with the intrusion of the microgranite (115 Ma; MacWilliam, 2018) and later the

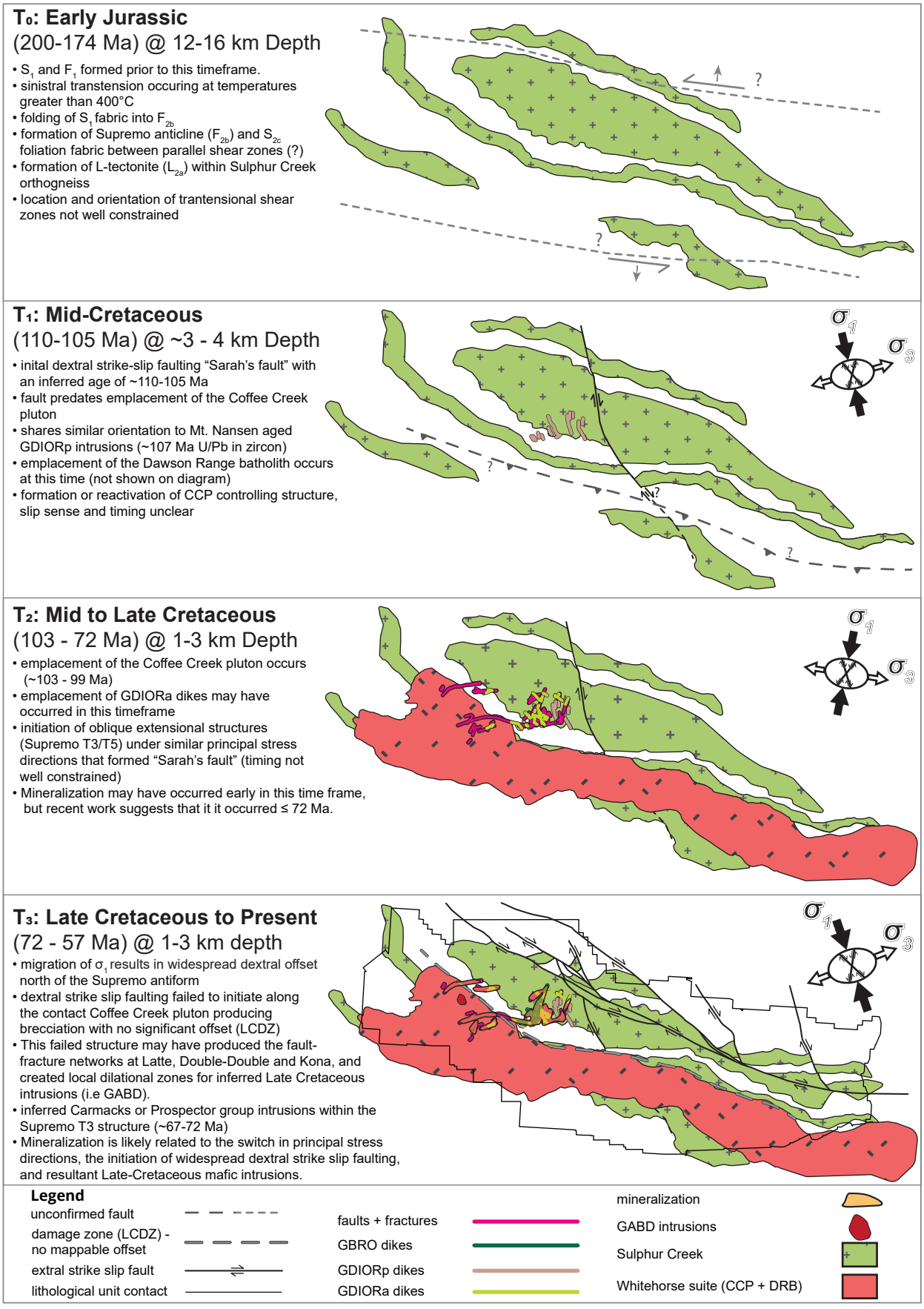


***Figure 25.*** *Simplified reconstruction of major rock-forming and deformational events at Coffee.*

porphyritic diorite (~107 Ma; this study) as they share a similar orientation. These first intrusive phases are approximately coincident with the orogen-scale shift in kinematics outlined by Nelson et al. (2013).

The CCP then intruded at approximately 103–99 Ma (MacWilliam, 2018), and the conjugate Supremo structures may have formed shortly after intrusion at $T_2$ under northeast-directed shortening (Fig. 25). This time of formation is compatible with the oldest possible age of mineralization (~96 Ma), as outlined in MacWilliam (2018). Data and inferences presented in this study, such as the mineralized inferred Late Cretaceous monzogabbro occurring in Supremo T3, suggest that the Supremo structures perhaps formed later in this $T_2$ window, closer to ~72–67 Ma (Figs. 20 and 25).

A change in the local stress regime after formation of the conjugate Supremo T-structures caused initiation of northwest-trending dextral strike-slip faults ($T_3$), as demonstrated by offset of bedrock units to the north and east of the Coffee deposit (Figs. 3 and 25). Minor brecciation also occurred along the LCDZ but failed to create observable offset of bedrock units. This minor movement on the LCDZ perhaps allowed for local dilation zones that accommodated both the inferred Late Cretaceous gabbroic intrusions and potentially mineralizing fluids. As the CCF system matured it continued to offset units, with ~25 km of demonstrable apparent dextral displacement (Figs. 3 and 25).

## Conclusions

The geochemical similarities between mineralized Coffee gabbroic dikes and plugs (GBRO and GABD; Plate 1) and Late Cretaceous volcanics (Fig. 19) suggest a potential Late Cretaceous age of mineralization. The structural analysis completed during this study has led to the interpretation that the depth of mineralization may be as shallow as 1 to 3 km, which is shallower than previously thought. Discovery of gabbroic diorite intrusions near the deposit provide a potential intrusive source of mineralizing fluids in the interpreted timeframe of gold deposition. The CCF may influence the emplacement of these interpreted Late Cretaceous mafic intrusions, similar to the BCF fault to the southeast. Known slip phases on the BCF (~73 Ma; Mottram et al., 2020) occur within the interpreted timeframe of gold deposition.

This study aligns with, and builds upon, previous interpretations that Coffee is a shallow, mid- to Late Cretaceous (~95–57 Ma; MacWilliam, 2018), low temperature (~200–250 °C; Buitenhuis, 2014; MacWilliam, 2018), structurally controlled gold-only deposit. In addition to classifying Coffee as an epizonal orogenic gold deposit, MacWilliam (2018) also suggested a connection between orogenic, (reduced) intrusion-related, and Carlin-like deposits, and noted that gold-only deposit models require critical assessment for the epizonal realm. Isotopic results presented by MacWilliam (2018) could possibly suggest a mixture of orogenic and igneous mineralizing fluid sources, which is an observation in agreement with interpretations of Carlin-type deposits (Muntean et al., 2011). This study outlines a potential connection between Coffee gold mineralization and inferred Late Cretaceous gabbroic intrusions, and further highlights similarities to fine-grained epizonal gold-only deposits such as low-sulphidation epithermal deposits and Carlin-like deposits.

## Future work

Additional work that may provide hard constraints on inferences made above and further understanding of the Coffee deposit are outlined below.

### Geochronology

Additional indirect age constraints on the timing of Coffee mineralization may be obtained by successfully dating the inferred Carmacks (or Prospector Mountain)-age intrusion or dikes using the U-Pb zircon method to get a maximum age. U-Pb dating of rutile or titanite that is intergrown with auriferous arsenian pyrite (MacWilliam, 2018) could provide a direct age of Coffee mineralization. Further $^{40}Ar/^{39}Ar$ dating of hydrothermal micas occurring strictly within mineralized dikes may build upon previous hydrothermal $^{40}Ar/^{39}Ar$ ages obtained by MacWilliam (2018) from within metamorphic bedrock, and could provide a more robust mica age separable from background CCP-related mica cooling ages. Additionally, U-Pb dating of post-mineral quartz-carbonate stockworks and breccias may provide a more precise minimum age of mineralization. The Paleogene population of Ap U-Pb dates in H689003 warrants additional work, perhaps in concert with existing Low-T thermochronologic datasets in the region.

### Breccia characterization

Previous studies outlined hypogene wallrock replacement ore in great detail, with moderate coverage of hypogene breccia phases (e.g., MacKenzie et al., 2013; Buitenhuis et al., 2015; MacWilliam, 2018). A detailed study of a broad assortment of hypogene and supergene breccia phases may clarify ore fluid-brecciation paragenesis and elucidate the nature of primary ore-forming structures relative to overprinted late-stage brecciation. Clumped isotope analysis of carbonate breccia matrices may help to determine matrix fluid temperatures and differentiate cryptic differences in hypogene structures.

### Uplift and exhumation

A more precise estimate of the depth of emplacement of the CCP and DRB, accompanied by ongoing low temperature thermochronology studies may further detail on the exhumation history of the region, as suggested by MacWilliam (2018).

### Metal zonation

The newly mapped unexposed intrusions on the Coffee property present a previously unrecognized potential influence on mineralization and alteration. Re-examination of potential alteration and metal zonation at the deposit scale as well as at smaller scales adjacent to the intrusions is warranted. Using four-acid digestion geochemical datasets recently adopted at the Coffee Project may assist with clarifying otherwise cryptic signatures potentially caused by the intrusions.

### Structural mapping

The newly discovered L-tectonite fabric within the upper Sulphur Creek unit on the Coffee property may have implications for regional tectonics in the Jurassic. Oriented rock sampling and other detailed structural mapping may be undertaken to improve understanding of this period of deformation in the YTT.

## Acknowledgments

The authors would like to thank Kathryn MacWilliam and previous authors who studied the Coffee Project, and acknowledge their significant geoscience contributions, without which the project would not be understood as it is today. We'd also like to thank Patrick Sack and

Maurice Colpron at the Yukon Geological Survey for their continued support and guidance with this study. Lastly, we'd like to thank the exploration team at the Coffee Project for all of their contributions and hard work that led to the current understanding of the deposit: Sarah Ellis, Logan Boyce, Nick Ryan, Aedan O'Brien, Connor Lyons, Davin Hofmann, George Sherlock and Braden Armstrong.

## References

Allan, M.M., Mortensen, J.K., Hart, C.J.R., Bailey, L.A., Sánchez, M.G., Ciolkiewicz, W., McKenzie, G.G. and Creaser, R.A., 2013. Magmatic and metallogenic framework of west-central Yukon and eastern Alaska. In: Tectonics, Metallogeny, and Discovery: The North American Cordillera and Similar Accretionary Settings, M. Colpron, T. Bissig, B. Rusk and J. Thompson (eds.), Society of Economic Geologists, Special Publication vol. 17, p. 111-168, https://doi.org/10.5382/SP.17.04.

Allmendinger, R., 2023. Mohr plotter and Stereonet; software from: Rick Allmendinger's Stuff. https://www.rickallmendinger.net/ [accessed 2023/05/05].

Angelier, J., 1975. Sur l'analyse de mesures recueillies dans des sites faillés: l'utilité d'une confrontation entre les méthodes dynamiques et cinématiques. Comptes Rendus de l'Académie des Sciences de Paris, vol. 281, no. 0023, p. 1805-1808.

Bailey, L., 2013. Late Jurassic fault-hosted gold mineralization of the Golden Saddle deposit, White Gold District, Yukon Territory. Unpublished MSc thesis, The University of British Columbia, British Columbia, Canada, 189 p.

Bartlett, S., 2016. Geology, alteration, and mineralization of the Sugar gold prospect, Yukon Territory, Canada. Unpublished BSc thesis, The University of British Columbia, British Columbia, Canada, 64 p.

Bartlett, S.E., Allan, M.M., Buitenhuis E.N., Smith, T.R. and Hart, C.J.R., 2016. Field investigations of the Sugar gold prospect, Dawson Range, Yukon (NTS 115J/14 and 115J/15). In: Yukon Exploration and Geology 2015, K.E. MacFarlane and M.G. Nordling (eds.), Yukon Geological Survey, p. 1-16.

Bishop, A. W., 1966. The strength of soils as engineering materials. Géotechnique, vol. 16, no. 2, p. 91-130.

Boyce, L., 2014. A paragenetic model and geochemistry of the Double-Double gold zone, Kaminak's Coffee gold project, Yukon, Canada. Unpublished B.Sc. thesis, The University of Alberta, Alberta, Canada, 85 p.

Buitenhuis, E., 2014. The Latte gold zone, Kaminak's Coffee gold project, Yukon, Canada: Geology, geochemistry, and metallogeny. Unpublished MSc thesis, The University of Western Ontario, Ontario, Canada, 197 p.

Buitenhuis, E., Boyce, L. and Finnigan, C., 2015. Advances in the mineralization styles and petrogenesis of the Coffee gold deposit, Yukon. In: Yukon Exploration and Geology 2014, K.E. MacFarlane, M.G. Nordling and P.J. Sack (eds.), Yukon Geological Survey, p. 29-43.

Cairnes, D.D., 1917. Investigations and mapping in Yukon Territory. In: Summary Report of the Geological Survey, Sessional Paper No. 26, 1917. Taché J. de L. (printer) and Platenaude, Es. L. (Minister of Mines), 419 p.

Cairnes, D.D., Boyd, W.H., Senécal, C.O. and Braidwood, A., 1917. Map 154 A, Southwestern Yukon. Geological Survey of Canada, geology map 154A, scale 1:506 880.

Cairnes, D.D., Senécal, C.O. and Fortin, J.O., 1918. Klotassin, Yukon Territory. Geological Survey of Canada, geology map, publication no. 1702, scale 1:126 720.

Casselman, S.C. and Brown, H., 2017. Casino porphyry copper-gold-molybdenum deposit, central Yukon (Yukon MINFILE 115J028). In: Yukon Exploration and Geology Overview 2016, K.E. MacFarlane (ed.), Yukon Geological Survey, p. 61-74, plus digital appendices.

Chartier, D., Couture, J.F., Sim, R. and Starkey, J., 2013. Mineral Resource Evaluation, Coffee Gold Project, Yukon, Canada. NI 43-101 technical report prepared by SRK Consulting Inc., Sim Geological Inc. and Starkey & Associates Inc. for Kaminak Gold Corp. Signed January 10, 2013, 217 p.

Colpron, M., Nelson, J. and Murphy, D., 2006. Tectonostratigraphic framework for the pericratonic terranes of the northern Canadian Cordillera. In: Paleozoic Evolution and Metallogeny of Pericratonic Terranes at the Ancient Pacific Margin of North America, Canadian and Alaskan Cordillera, M. Colpron and J. Nelson (eds.), Geological Association of Canada Special Paper 45, p. 1-23.

Colpron, M., Sack, P.J., Crowley, J.L., Beranek, L.P. and Allan, M.M., 2022. Late Triassic to Jurassic magmatic and tectonic evolution of the Intermontane terranes in Yukon, northern Canadian Cordillera: Transition from arc to syn-collisional magmatism and post-collisional lithospheric delamination. Tectonics, vol. 41, issue 2, e2021TC007060, https://doi.org/10.1029/2021TC007060.

Cox, S.F., 2020. Chapter 2: The dynamics of permeability and fluid flow in overpressured, fracture-controlled hydrothermal systems. In: Applied Structural Geology of Ore-Forming Hydrothermal Systems, J.V. Rowland and D.A. Rhys (eds.) Society of Economic Geologists, vol. 21, https://doi.org/10.5382/rev.21.02.

Cruikshank, P., 2011. Hydrothermal alteration and gold mineralization of the Supremo zone, Coffee property, Yukon, Canada. Unpublished BSc thesis, The University of Western Ontario, Ontario, Canada, 67 p.

Doerksen, G., Pilotto, D., McLeod, K., Sim, R., Levy, M., Sharp, T., Smith, M.E. and Kappes, D.W., 2016. NI 43-101 Feasibility Study Technical Report for the Coffee Gold Project, Yukon Territory, Canada. NI 43-101 technical report prepared by JDS Energy and Mining Inc. for Kaminak Gold Corp. Effective date: February 18, 2016, 460 p.

Fossen, H., Teyssier, C. and Whitney, D. L., 2013. Transtensional folding. Journal of Structural Geology, vol. 56, p. 89-102, https://doi.org/10.1016/j.jsg.2013.09.004.

Friend, M., 2022. Tectonomagmatic framework for Late Cretaceous postsubduction magmatism in west-central and southern Yukon. Unpublished MSc thesis, The University of British Columbia, British Columbia, Canada, 531 p.

Friend, M.A., Allan, M.M. and Hart, C.J.R., 2018. New contributions to the bedrock geology of the Mount Freegold district, Dawson Range, Yukon (NTS 115I/2, 6 and 7). In: Yukon Exploration and Geology 2017, K.E. MacFarlane (ed.), Yukon Geological Survey, p. 47-68.

Frost, R.B., Barnes, C.G., Collins, W.J., Arculus, R.J., Ellis, D.J. and Frost, C.D., 2001. A Geochemical Classification for Granitic Rocks. Journal of Petrology, vol. 42, no. 11, p. 2033-2048.

Gaboury, D., 2019. Parameters for the formation of orogenic gold deposits. Applied Earth Science: Transactions of the Institutions of Mining and Metallurgy, vol. 128, issue 3, p. 124-133, https://doi.org/10.1080/25726838.2019.1583310.

Groves, D.I., Santosh, M. and Zhang, L., 2020. A scale-integrated exploration model for orogenic gold deposits based on a mineral system approach. Geoscience Frontiers, vol. 11, issue 3, p. 719-738, https://doi.org/10.1016/j.gsf.2019.12.007.

Harrison, T.M. and Zeitler, P.K., 2005. Fundamentals of Noble Gas Thermochronometry. Reviews in Mineralogy and Geochemistry, vol. 58, no. 1, p. 123-149.

Hastie, A.R., Kerr, A.C., Pearce, J.A. and Mitchell, S.F., 2007. Classification of altered volcanic island arc rocks using immobile trace elements: Development of the Th-Co discrimination diagram. Journal of Petrology, vol. 48, issue 12, p. 2341-2357, https://doi.org/10.1093/petrology/egm062.

Hollister, L.S., Grissom, G.C., Peters, E.K., Stowell, H.H. and Sisson, V.B., 1987. Confirmation of the empirical correlation of Al in hornblende with pressure of solidification of calc-alkaline plutons. American Mineralogist, vol. 72, p. 231-239.

Jaworski, B.J. and Meyer, B., 2000. Geological and geochemical report on the Coffee Creek intrusion-related gold target, west central Yukon Territory. Yukon Energy, Mines and Resources Assessment Report 094064, 42 p.

Jaworski, B. and Vanwermeskerken, M., 2001. Geological and geochemical report on the Coffee Creek intrusion-related gold target, west central Yukon Territory. Yukon Energy, Mines and Resources Assessment Report 094207, 53 p.

Johnston, S.T., 1999. Large-scale coast-parallel displacements in the Cordillera: a granitic resolution to a paleomagnetic dilemma. Journal of Structural Geology, vol. 21, issue 8-9, p. 1103-1108, https://doi.org/10.1016/S0191-8141(99)00015-2.

Johnston, S.T., Wynne, P.J., Francis, D., Hart, C.J.R., Enkin, R.J. and Engebretson, D.C., 1996. Chemical analyses for lavas of the Carmacks group, Yukon Canada. In: Yellowstone in Yukon: The Late Cretaceous Carmacks Group. Geology vol. 24 no. 11, https://doi.org/10.1130/0091-7613(1996)024%3C0997:YIYTLC%3E2.3.CO;2.

Joyce, N.L., 2002. Geologic setting, nature, and structural evolution of intrusion-hosted Au-bearing quartz veins at the Longline occurrence, Moosehorn Range area, west-central Yukon Territory. Unpublished MSc thesis, The University of British Columbia, British Columbia, Canada, 199 p.

Kitchen, J.G., Essman, J.E., Brubacher, A.D. and Johansson, P., 2025. Bedrock geology map of the Coffee Project, Dawson Range, Yukon (parts of NTS 115J/13, 14 and 15). Yukon Geological Survey, Government of Yukon, Open File 2025-5, scale 1:50 000.

Klöcking, M., Mills, L., Mortensen, J. and Roots, C., 2016. Geology of mid-Cretaceous volcanic rocks at Mount Nansen, central Yukon, and their relationship to the Dawson Range batholith. Yukon Geological Survey, Open File 2016-25, 37 p.

Kovacs, N., Allan, M.M., Crowley, J.L., Colpron, M., Hart, C.J.R., Zagorevski, A. and Creaser, R.A., 2020. Carmacks Copper Cu-Au-Ag deposit: Mineralization and postore migmatization of a Stikine arc porphyry copper system in Yukon, Canada. Economic Geology, vol. 115, no.7, p. 1413-1442, https://doi.org/10.5382/econgeo.4756.

Kuiper, Y.D., Murray, D.P., Ellison, S. and Crowley, J.L., 2022. U-Pb detrital zircon analysis of sedimentary rocks of the southeastern New England Avalon terrane in the U.S. Appalachians: Evidence for a separate crustal block. In: New Developments in the Appalachian-Caledonian-Variscan Orogen, Y.D. Kuiper, J.B. Murphy, R.D. Nance, R.A. Strachan and M.D. Thompson (eds.), Geological Society of America, Special Paper, vol. 554, https://doi.org/10.1130/SPE554.

Le Maitre, R. W. (1989). A Classification of Igneous Rocks and Glossary of Terms. Recommendations of the IUGS Commission on the Systematics of Igneous Rocks. Oxford: Blackwell.

Lee, W., 2017. A Petrographic and fluid inclusion comparison of mid-Cretaceous gold bearing veins near the 5 Moz Coffee deposit, west-central Yukon. Unpublished BSc thesis, The University of British Columbia, British Columbia, Canada, 102 p.

Lisle, R.J., Orife, T.O., Arlegui, L., Liesa, C. and Srivastava, D., 2006. Favoured states of palaeostress in the Earth's crust: evidence from fault-slip data. Journal of Structural Geology, vol. 28, issue 6, p. 1051-1066, https://doi.org/10.1016/j.jsg.2006.03.012.

MacKenzie, D., Craw, D. and Finnigan, C., 2013. Structural controls on alteration and mineralization at the Coffee gold deposits, Yukon. In: Yukon Exploration and Geology 2013, K.E. MacFarlane, M.G. Nordling, and P.J. Sack (eds.), Yukon Geological Survey, p. 119-131.

MacKenzie, D., Craw, D. and Finnigan, C., 2014. Lithologically controlled invisible gold, Yukon, Canada. Mineralium Deposita, vol. 50, p.141-157, https://doi.org/10.1007/s00126-014-0532-5.

MacWilliam, K. R., 2018. The geology and genesis of the Coffee gold deposit in west-central Yukon, Canada: Implications for the structural, magmatic, and metallogenic evolution of the Dawson Range, and gold exploration models. Unpublished PhD thesis, The University of British Columbia, British Columbia, Canada, 497 p.

McCausland, P.J., Symons, D.T., Hart, C.J. and Blackburn, W.H., 2006. Assembly of the northern Cordillera: new paleomagnetic evidence for coherent, moderate Jurassic to Eocene motion of the Intermontane Belt and Yukon-Tanana terranes. In: Paleogeography of the northern Cordillera: evidence for and against large-scale displacements, J.W. Haggart, R.J. Enkin and J.W.H. Monger (eds.), Geological Association of Canada, p. 147-170.

McKenzie, G.G., Allan, M.M., Mortensen, J.K., Hart, C.J.R., Sánchez, M. and Creaser, R.A., 2013. Mid-Cretaceous orogenic gold and molybdenite mineralization in the Independence Creek area, Dawson range, parts of NTS 115J/13 and 14. In: Yukon Exploration and Geology 2012, K.E. MacFarlane, M.G. Nordling and P.J. Sack (eds.), Yukon Geological Survey, p. 73-97.

Middlemost, E.A.K., 1994. Naming materials in the magma/igneous rock system. Earth-Science Reviews, vol. 37, issues 3-4, p. 215-224, https://doi.org/10.1016/0012-8252(94)90029-9.

Mottram, C.M., Kellett, D.A., Barresi, T., Zwingmann, H., Friend, M., Todd, A. and Percival, J.B., 2020. Syncing fault rock clocks: Direct comparison of U-Pb carbonate and K-Ar illite fault dating methods. The Geological Society of America, vol. 48, no. 12, p. 1179-1183, https://doi.org/10.1130/G47778.1.

Muntean, J.L., Cline, J.S., Simon, A.C. and Longo, A.A., 2011. Magmatic-hydrothermal origin of Nevada's Carlin-type gold deposits. Nature Geoscience, vol. 4, p. 122-127, doi: 10.1038/NGEO1064.

Nelson, J.L., Colpron, M. and Israel, S., 2013. The Cordillera of British Columbia, Yukon, and Alaska: Tectonics and metallogeny. In: Tectonics, metallogeny and discovery: the North American cordillera and similar accretionary settings, M. Colpron, T. Bissig, B.G. Rusk and J.F.H. Thomson (eds.), Society of Economic Geologists, Special Publication, vol. 17, p. 53-109.

Newmont Corporation, 2023. Newmont 2023 reserves and resources results. News release, 16 p. https://www.newmont.com/investors/reports-and-filings/default.aspx. [accessed 2024/12/30].

Passchier, C.W. and Trouw, R.A.J., 1996. Micro-tectonics. Springer-Verlag, New York, 366 p.

Richards, J.P., Spell, T., Rameh, E., Razique, A. and Fletcher, T., 2012. High Sr/Y magmas reflect arc maturity, high magmatic water content, and porphyry Cu +/- Mo +/- Au potential: Examples from the Tethyan arcs of Central and eastern Iran and western Pakistan, Economic Geology, vol. 107, p. 310, https://doi.org/10.2113/econgeo.107.2.295.

Ryan, J.J., Zagorevski, A., Williams, S.P., Roots, C., Ciolkiewicz, W., Hayward, N. and Chapman, J.B., 2013a. Geology, Stevenson Ridge (northeast part), Yukon; Geological Survey of Canada, Canadian Geoscience Map 116 (2nd edition, preliminary), scale 1:100 000, doi:10.4095/292407.

Ryan, J.J., Zagorevski, A., Williams, S.P., Roots, C., Ciolkiewicz, W., Hayward, N. and Chapman, J.B., 2013b. Geology, Stevenson Ridge (northeast part), Yukon; Geological Survey of Canada, Canadian Geoscience Map 117 (preliminary), scale 1:100 000, doi:10.4095/292372.

Ryan, S., 2007. Geochemical - Geophysical report of Coffee claims 1-112, NTS 115J/14. Yukon Energy, Mines and Resources Assessment Report 094932, 55 p.

Ryan, S., 2008. Geochemical – Geophysical report of Coffee claims 1-112, NTS 115J/14. Yukon Energy, Mines and Resources Assessment Report 095219, 265 p.

Sánchez, M.G., Allan, M.M., Hart, C. J.R. and Mortensen, J.K., 2014. Structural control of mineralization recognized by magnetite-destructive faults of the western Yukon and eastern Alaska Cordilleran hinterland. In: Geological Society of America 2014 annual meeting Abstracts with Programs, vol. 46, no. 6, p.462.

Selby, D. and Creaser, R.A., 2001. Late and mid-Cretaceous mineralization in the northern Canadian Cordillera: Constraints from Re-Os molybdenite dates. Economic Geology vol. 96, no. 6, p. 1461-1467, https://doi.org/10.2113/gsecongeo.96.6.1461.

Sibson, R.H., 2003. Thickness of the Seismic Slip Zone. Bulletin of the Seismological Society of America, vol. 93, no. 3, p. 1169-1178, https://doi.org/10.1785/0120020061.

Šilerová, D., Dyck, B., Cutts, J.A. and Larson, K., 2023 . Long-lived (180 Myr) ductile flow within the Great Slave Lake shear zone. Tectonics, vol. 42, issue 9, https://doi.org/10.1029/2022TC007721.

Sláma, J., Košler, J., Condon, D.J., Crowley, J.L., Gerdes, A., Hanchar, J.M., Horstwood, M.S.A., Morris, G.A., Nasdala, L., Norberg, N., Schaltegger, U., Schoene, B., Tubrett, M.N and Whitehouse, M.J., 2008. Plešovice zircon - A new natural reference material for U-Pb and Hf isotopic microanalysis. Chemical Geology, vol. 249, issues 1-2, p. 1-35, https://doi.org/10.1016/j.chemgeo.2007.11.005.

Staples, R.D., Gibson, H.D., Colpron, M. and Ryan, J.J., 2016. An orogenic wedge model for diachronous deformation, metamorphism, and exhumation in the hinterland of the northern Canadian Cordillera. Lithosphere, vol. 8, no. 2, p. 165–184, https://doi.org/10.1130/L472.1.

Stüwe, K., Will, T.M. and Zhou, S., 1993. On the timing relationship between fluid production and metamorphism in metamorphic piles: Some implications for the origin of post-metamorphic gold mineralisation. Earth and Planetary Science Letters, vol. 114, issue 4, p.417-430, https://doi.org/10.1016/0012-821X(93)90073-I.

Sun, S.S. and McDonough, W.F., 1989 . Chemical and isotopic systematics of oceanic basalts: implications for mantle composition and processes. Geological Society, London, Special Publications, vol. 42, p. 313-345, https://doi.org/10.1144/GSL.SP.1989.042.01.19.

Tempelman-Kluit, D.J., 1973a. Map 16-1973, Snag, Yukon Territory. Geological Survey of Canada, geology map 16-1973 (115 K-J), scale 1:250 000.

Tempelman-Kluit, D.J., 1973b. Reconnaissance geology of Aishihik Lake, Snag, and part of Stewart River map-areas, west-central Yukon. Geological Survey of Canada, paper 73-4, 97 p.

van Drecht, L.H., Beranek, L.P., Colpron, M. and Wiest, A.C., 2022. Development of the Whitehorse trough as a strike-slip basin during Early to Middle Jurassic arc-continent collision in the Canadian Cordillera: Geosphere, vol. 18, no. 5, p. 1538–1562, https:// doi.org /10.1130 /GES02510.1.

Wainwright, A.J., Simmons, A.T., Finnigan, C.S., Smith, T.R. and Carpenter, R.L., 2011. Geology of new gold discoveries in the Coffee Creek area, White Gold district, west-central Yukon. In: Yukon Exploration and Geology 2010, K.E. MacFarlane, L.G. Weston, and C. Relf (eds.), Yukon Geological Survey, p. 233-247.

Widenbeck, M., Allé, P., Corfu, F., Griffin, W.L., Meier, M., Oberli, A., von Quadt, A., Roddick, J.C. and Spiegel, W., 1995. Three natural zircon standards for U-Th-Pb, Lu-Hf, trace element and REE Analyses. Geostandards Newsletter, vol. 19, issue 1, p. 1-23, https://doi.org/10.1111/j.1751-908X.1995.tb00147.x.

Yukon Geological Survey, 2023a. Yukon digital bedrock geology. Yukon Geological Survey, https://yukon.ca/en/yukon-geology#bedrock-geology, [accessed 2024/09/15].

Yukon Geological Survey, 2023b. Yukon Geochronology – A database of Yukon isotopic age

determinations. Yukon Geological Survey, http://data.geology.gov.yk.ca/Compilation/23 [accessed 2024/09/15].

Yukon Geological Survey, 2023c. A digital atlas of terranes for the northern Cordillera. Yukon Geological Survey, https://data.geology.gov.yk.ca/Compilation/2 [accessed 2024/03/15].

# Appendices (digital files)

## Appendix A

Zircon U-Pb geochronology methodology.

## Appendix B

Zircon U-Pb geochronology data.

## Appendix C

Apatite U-Pb geochronology data.

## Appendix D

Whole-rock geochemistry data for select Coffee intrusions shown in Figures 19 and 20.

Yukon Geological Survey
Energy, Mines and Resources
Government of Yukon